



# Evaluation of tectonic activity in the Kopongo area, southwestern Cameroon: insights from geomorphic indices, remote sensing, and GIS

Thierry Abou'ou Ango<sup>1,2</sup> · Mero Yannah<sup>3</sup> · Rachid El Hamdouni<sup>4</sup> · Bernard Njom<sup>1</sup> · Joseph Mvondo Ondoa<sup>1</sup>

Received: 24 April 2022 / Accepted: 24 January 2023 / Published online: 15 February 2023  
© Saudi Society for Geosciences and Springer Nature Switzerland AG 2023

## Abstract

Geomorphologic investigations were undertaken in the Kopongo region, located in the northwestern margin of the Congo craton. The study carry out on the Kopongo, a portion of the Cameroonian passive margin (3°53'–4°05'N, 10°06'–10°19'E), aims to examine the topographic and hydrographic anomalies through the use of geomorphic indices combined with geographic information systems, field observations, and literature data for the categorization of the relative index of active tectonics. Geomorphic and morphotectonic evaluations of this area have been carried out by implicating different geomorphic indices such as hypsometric parameters, relative tectonic uplift, basin shape, asymmetry factor, bifurcation ratio, and valley floor width to valley height ratio. The results obtained show that the region includes areas of high (14.89%), moderate (72.71%), and low (12.33%) tectonic activity zones. This inequitable distribution of the relative tectonic activity is caused by variations of tectonic uplift (0.16–0.68) and tilting (0.06–35.6). A strong correlation is seen between structural patterns and field morphotectonic indices such as river and channel anomalies, V-shaped valleys, hill tiltings, and young topographies. This indicates an influence of neotectonic uplift rates dating from the Cretaceous to the Quaternary. The origin of neotectonics along this passive margin correlates with the high volcanic activity along the Cameroon Volcanic Line, which is a consequence of the mechanical behavior of the lithosphere beneath West-Central Africa. The Kopongo area is more influenced by high and moderate tectonic activity. Thus, it appears that this area has been rejuvenated due to interactions with climate, lithology, and neotectonic activities.

**Keywords** Nyong Group · Kopongo · Active tectonics · Uplift rates · Tilting · Geomorphic indices

## Introduction

The genesis of landscape features at the regional and local scales is interplayed among climatic conditions, geological formations, and past and recent geological events. Therefore,

the used of geophysical data, satellite images, and geomorphic anomalies in various geodynamic contexts is applied to evaluate tectonic activity (El Hamdouni et al. 2008; Amine et al. 2020; Ezati et al. 2021). Otherwise, the tectonic evolution of any drainage system morphologies shows that rivers and topography with their recognizable patterns correspond to new analytical and modeling tools used for the study of tectonic which is active. After the success of geodesic and dating methods, morphotectonic analysis, structural geology, and seismology are other methods used in the acquisition of anomalies from tectonic, it conclude uplift, incision, and erosion rates (e.g., Burbank and Anderson 2001; El Hamdouni et al. 2008; Bathrellos et al. 2009). The processing and analysis of geomorphic indices at different scales and environments played an important role in the investigation of landscape and river systems (e.g., Bahrami et al. 2020; Abou'ou Ango et al. 2021).

Currently situated in the southwestern part of Cameroon, the Kopongo site is developed within the Western Central

---

Responsible Editor: Stefan Grab

✉ Thierry Abou'ou Ango  
abououangothierry@yahoo.fr

- <sup>1</sup> Department of Earth Sciences, Faculty of Science, University of Yaounde I, P.O. Box 812, Yaounde, Cameroon
- <sup>2</sup> Compagnie Minière du Cameroun, BP 35561, Yaoundé, Cameroun
- <sup>3</sup> Institut de Recherches Géologiques Et Minières, BP 4110 Nlongkak, Yaoundé, Cameroun
- <sup>4</sup> Department of Civil Engineering, ETSICCP, University of Granada, Campus Fuentenueva S/N, 18071 Granada, Spain

African region well-known as a sedimentary unit deposited along a humid passive margin portion (Owona 2008). Due to the lack of a full suite seismotectonic landscape data in the numerous localities worldwide, it is evident that many researchers are using multiple geomorphic indices in order to measure, identify, and delineate regions of anomalously low to high deformation rates. At the south-western regions of Cameroon, these seismic activities occur along or close to the major tectonic structures and the Cameroon Volcanic Line (Fig. 1c; Gaelle Nana et al. 2021; Ndibi et al. 2021).

The quantitative analysis reported here constitutes significant investigations through geomorphologic indices (Tables 1 and 2) and fieldwork in order to improve the understanding of the tectonic control, the role played by lithologic variability, and climatic changes on the evolution of the landscape in Kopongo. Several reports have shown the importance of using geophysical data, satellite images, and geomorphic anomalies in various geodynamic contexts to evaluate tectonic activity (El Hamdouni

et al. 2008; Amine et al. 2020; Ezati et al. 2021). However, the tectonic evolution of any drainage system morphologies shows that rivers and topography with their recognizable patterns correspond to new analytical and modeling tools used for the study of active tectonics. After the success of geodesic and dating methods, morphotectonic analysis, structural geology, and seismology are other methods used in the acquisition of anomalies from tectonic, conclude uplift, incision, and erosion rates (e.g., Burbank and Anderson 2001; El Hamdouni et al. 2008; Bathrellos et al. 2009). The processing and analysis of geomorphic indices at different scales and environments played an important role in the investigation of landscape and river systems (e.g., Bahrami et al. 2020; Abou’ou Ango et al. 2021).

Currently situated in the southwestern part of Cameroon, the Kopongo site is developed within the Western Central African region well-known as a sedimentary unit deposited along a humid passive margin portion (Owona 2008). Due to the lack of a full suite of seismotectonic landscape data

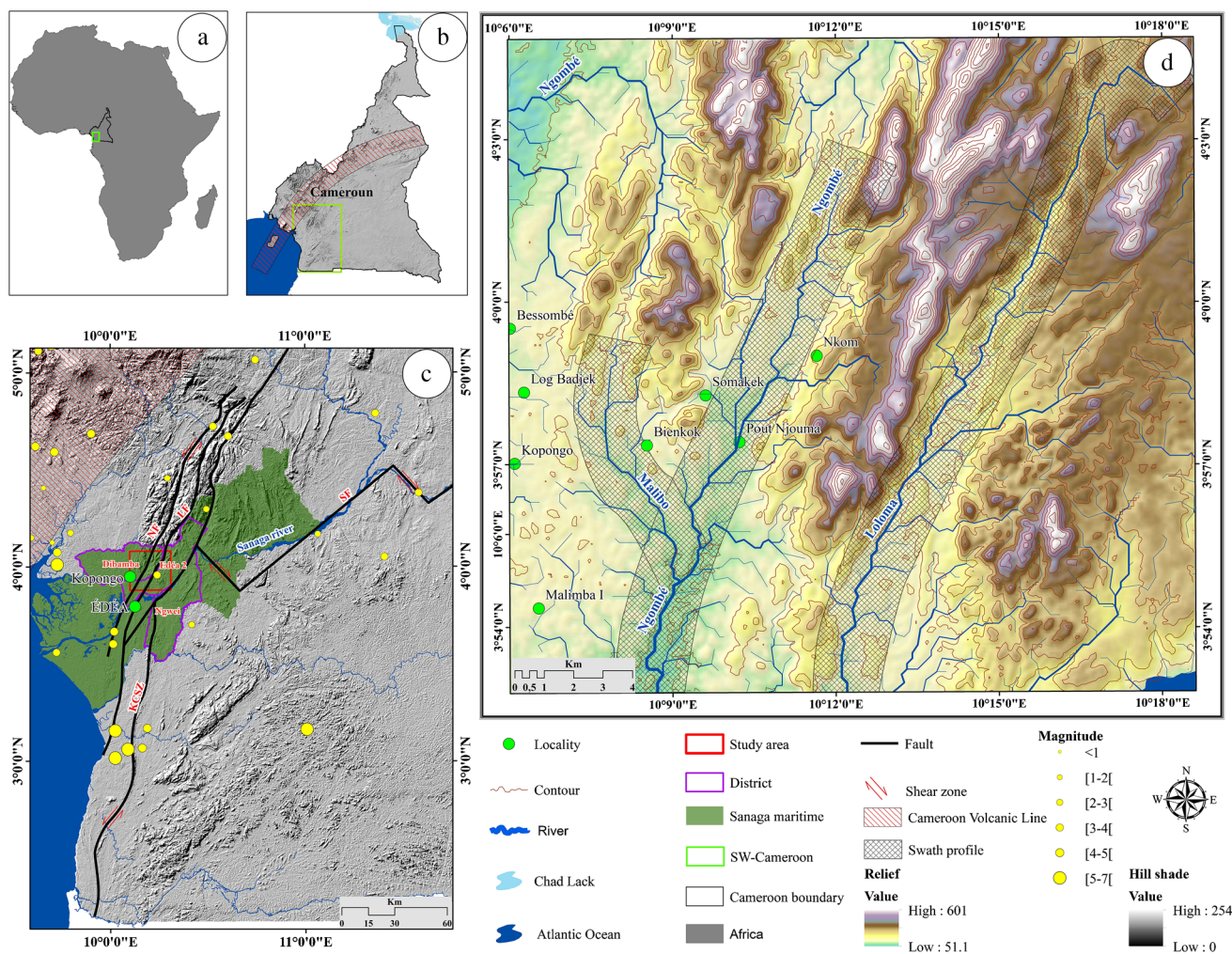


**Fig. 1** Kopongo geographical position: **a** map illustrating Africa and Cameroon. **b** Cameroon. **c** SW-Cameroon with the Kopongo sub-divisions; LF, Loloma fault; NF, Ngombe fault; SF, Sanaga fault; and KCSZ, Kribi Campo Shear Zones. **d** Kopongo area

**Table 1** Formulas used for the calculation of geomorphic indices using previous literature

No	Parameters	Symbol	Formula	Classes	References
1	Hypsometric integral	Hi	$Hi = (Z_{\text{mean}} - Z_{\text{min}}) / (Z_{\text{max}} - Z_{\text{min}})$ , Where, $Z_{\text{max}}$ = maximum height of the basin (m), $Z_{\text{min}}$ = minimum height,	<ul style="list-style-type: none"> <li>*Class 1: <math>0.55 &lt; Hi &lt; 1</math>, high tectonic activity;</li> <li>*Class 2: <math>0.45 &lt; Hi &lt; 0.55</math>, moderate tectonic activity;</li> <li>*Class 3: <math>0 &lt; Hi &lt; 0.45</math>, low tectonic activity/inactive</li> </ul>	El Hamdouni et al. 2008
2	Hypsometric curve	Hc	/	<ul style="list-style-type: none"> <li>* Corresponds to the percentage of surface area above a certain height;</li> <li>* Is the ratio between the relative height (h/H, total basin height ratio) and the relative area (a/A, total basin area ratio) of the watershed;</li> <li>* A convex hypsometric curve indicates active young watershed associated to weak erosional effects;</li> <li>* S-shaped curves show the areas under influence of the moderate erosional processes;</li> <li>* Concave curves express old watersheds associated with strong erosional processes (Fig. 4a–c)</li> </ul>	Keller and Pinter 1996
3	Relative tectonic uplift index	U	$U = Z_m + (1 - Hi)$ Where, $Z_m$ is considered the average height of the sub-watershed obtained from the elevation covering 50% of the area and normalized to the maximum elevation of the main watershed	<ul style="list-style-type: none"> <li>* Class 1: <math>U &gt; 0.6</math>, very high tectonic uplift;</li> <li>* Class 2: <math>0.3 &lt; U &lt; 0.6</math>, high tectonic uplift;</li> <li>* Class 3: <math>U &lt; 0.3</math>, moderate to low tectonic uplift or mild subsidence</li> </ul>	Ajay kumar et al. 2017
4	Basin shape	Bs	$Bs = Bl/Bw$ Where Bl and Bw correspond to the maximum length, and the maximum width, respectively (Fig. 4g)	<ul style="list-style-type: none"> <li>*Class 1: <math>1.77 &lt; Bs &lt; 3.22</math>, elongated in nature, high tectonic activity;</li> <li>* Class 2: <math>1.21 \leq Bs \leq 1.76</math>, elongated to sub-elongated in nature, moderate tectonic activity;</li> <li>*Class 3: <math>1.11 &lt; Bs &lt; 1.20</math>, more circular in nature, low tectonic activity</li> </ul>	Mahmood and Glosguen 2012

**Table 2** Formulas used for the calculation of geomorphic indices using previous literature

No	Parameters	Symbol	Formula	Classes	References
1	Asymmetry factor	AF	$AF = 100(A_r/A_t)$ Where $A_t$ corresponds to the total area of a watershed while $A_r$ represents the area on the right side (facing downstream) of the main river in the watershed (Fig. 4d–f)	<ul style="list-style-type: none"> <li>* <math>AF &lt; 50</math>, suggests uplift processes affect the left sides of the river system;</li> <li>* <math>AF</math> equal or close to 50, shows that the region is stable;</li> <li>* <math>AF &gt; 50</math>, suggests uplift processes; influence the right side of the river system</li> </ul>	Keller and Pinter 2002
2	Asymmetry factor	$AF'$	$AF' =  50 - AF $	<ul style="list-style-type: none"> <li>* Class 1: <math>AF' &lt; 5</math>, symmetric watershed;</li> <li>* Class 2: <math>AF' = 5–10</math>, gently asymmetric watershed;</li> <li>* Class 3: <math>AF' = 10–15</math>, moderately asymmetric watershed;</li> <li>* Class 4: <math>AF' &gt; 15</math>, strongly asymmetric watershed</li> </ul>	Pérez-Peña et al. 2010
3	Bifurcation ratio	Rb	$Rb = Nu / Nu + 1$ Where, Rb is the bifurcation ratio, while Nu and Nu + 1 are the number of stream segments of a given order and the number of stream segments of next higher order, respectively	<ul style="list-style-type: none"> <li>* Class 1: <math>Rbm \geq 5</math>, high tectonic activity</li> <li>* Class 2: <math>3 &lt; Rbm &lt; 5</math>, moderate tectonic activity</li> <li>* Class 3: <math>Rbm &lt; 3</math>, low tectonic activity</li> </ul>	Chow Ven 1964
4	Ratio of valley floor width to valley height	Vf	$Vf = 2Vfw / (Eld + Erd - 2Esc)$ , Where Vfw and Esc are the width of the valley floor and the elevation of the valley floor, respectively, while Eld and Erd represent the elevations of the left and the right valley divides (facing downstream) respectively, (Fig. 4h)	<ul style="list-style-type: none"> <li>* Class 1: <math>Vf &lt; 0.5</math>, high tectonic activity</li> <li>* Class 2: <math>0.5 &lt; Vf &lt; 1.0</math>, moderate tectonic activity</li> <li>* Class 3: <math>Vf &gt; 1</math>, low tectonic activity</li> </ul>	Keller and Pinter 2002
5	Relative tectonic activity	IAT	$IAT = S/n$ , Where S represents the sum of all indices values, and n corresponds to their total number	<ul style="list-style-type: none"> <li>* Class 1: very high tectonic activity, <math>1.0 \leq IAT &lt; 1.5</math></li> <li>* Class 2: high tectonic activity, <math>1.5 \leq IAT &lt; 2.0</math></li> <li>* Class 3: moderate tectonic activity, <math>2.0 \leq IAT &lt; 2.5</math></li> <li>* Class 4: low tectonic activity, <math>IAT &gt; 2.5</math></li> </ul>	El Hamdouni et al. 2008

in the numerous localities worldwide, it is evident that many researchers are using multiple geomorphic indices to measure, identify, and delineate regions of anomalously low to high deformation rates. In the southwestern region of Cameroon, these seismic activities occur along or close to the major tectonic structures and the Cameroon Volcanic Line (Fig. 1c; Gaele Nana et al. 2021; Ndibi et al. 2021).

The quantitative analysis reported here constitutes the investigations through geomorphologic indices (Tables 1 and 2) and fieldwork to improve the understanding of the tectonic control, the role played by lithologic variability, and climatic changes on the evolution of the landscape in Kopongo. In this contribution, an assessment of the distribution and intensity of tectonic activities under multiple compressive and extensive stresses in the region was carried out for geodynamic understanding. Various geomorphic indices were used to evaluate relative rates of active tectonics (IAT)

and for classifying the sub-basins into different classes from relatively low to the highest tectonic activity.

## Geological, geomorphological, and climatic settings

### Geological setting

Kopongo area is located within the Paleoproterozoic Nyong Group (NyG) which crops out on the northwestern border of the Archean Congo craton in southern Cameroon (Fig. 2). This group constitutes the northwestern part of the reworked Archean Ntem Complex. It is documented as the reactivation of the northwestern corner of the Congo Craton during the Paleoproterozoic (Toteu et al. 1994; Weber et al. 2016; Bouyo Houketchang et al. 2019) and Neoproterozoic (Lasserre and



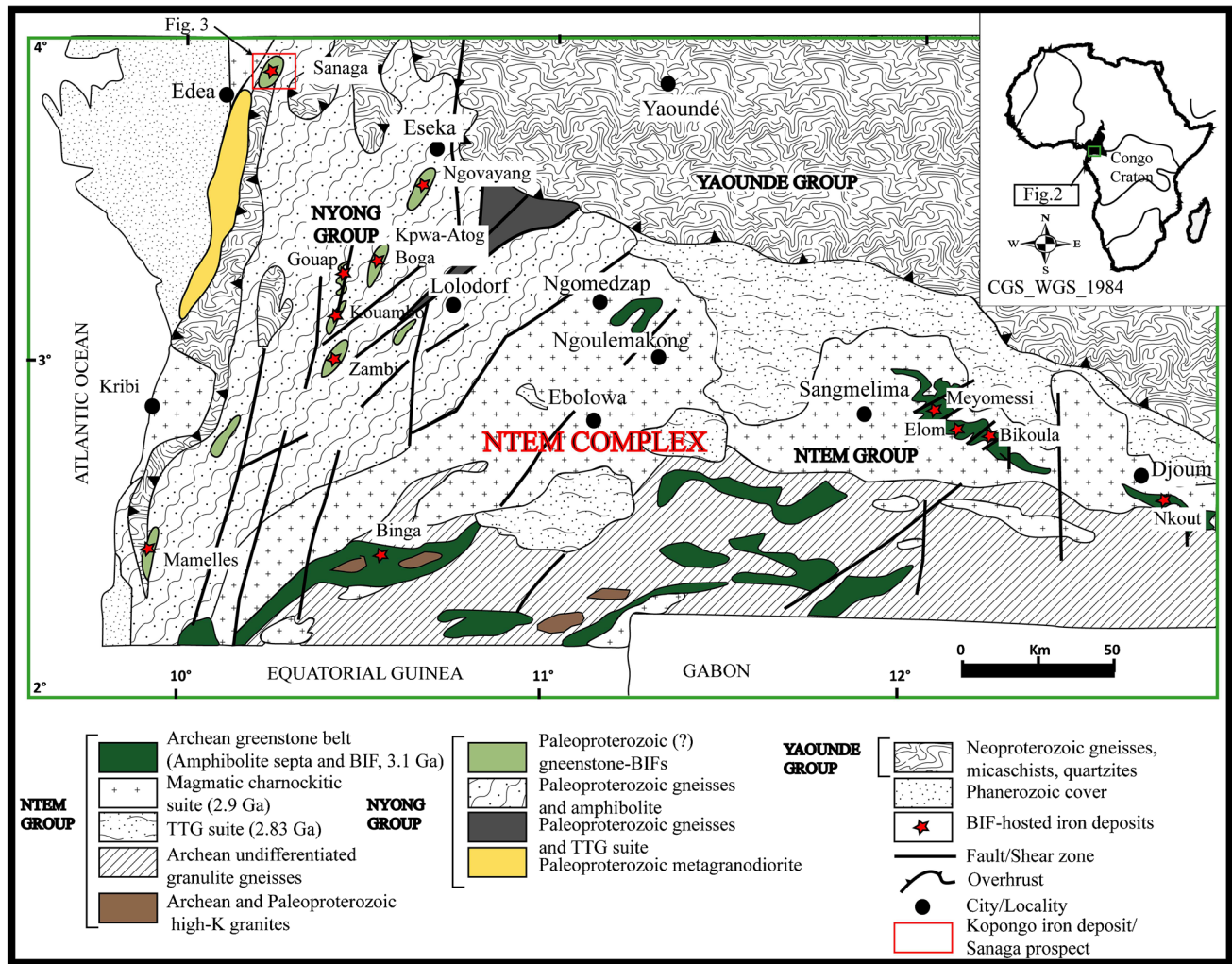


Fig. 2 Geological map of SW-Cameroon (modified after Maurizot et al. 1986)

Soba 1976; Toteu et al. 1990; Castaing et al. 1994) collisional events. The area consists of a Proterozoic basement (Maurizot et al. 1986) marked by slightly undulating and gentle topography as a result of extensive erosion during the Eburnean-Transamazonian (e.g., Loose and Schenk 2018), Neoproterozoic orogenies (e.g., Fuh et al. 2021), and present tectonic activities (e.g., Nsangou Ngapna et al. 2020). For the past decade, numerous studies within this passive margin have shown several reactivations related to regional structures such as Loloma, Ngombe, and Sanaga faults (Moussango Ibohn et al. 2018; Nsangou Ngapna et al. 2020), and Kribi Campo Shear Zones (KCSZ, Sandron et al. 2018) that surround and affect the Kopongo area (Fig. 1c). The west central African region is characterized by several geological features: Cretaceous Benue rifts, Tertiary Cameroon Volcanic Line (CVL), and Tertiary Adamawa volcanic uplift. They are the three active regional structures that generate high tectonic activities in the region (Cornacchia and

Dars 1983; Ngako et al. 1991; Déruelle et al. 2007; Moudi et al. 2007). However, this region is characterized by three large-scale major faults: the Centre Cameroon Shear Zone (CCSZ), the Kribi-Campo fault (KCF), and the Sanaga fault (SF).

Benue trough is a regional feature found on the western side of Kopongo and known to have formed at the same time during the lower Cretaceous and the opening of the Gulf of Guinea. It represents the continental prolongation of equatorial oceanic fracture zones along which a sinistral transcurrent shear occurred (Benkhelil and Robineau 1983). This feature has the same geometry as the CVL, defined by a N30°E trending intraplate “Y-shape” alkaline volcano-plutonic formations extending over 2000 km long and generally less than 200 km wide (Fig. 1b). It is a major African volcano-tectonic structure that dates from Cretaceous to present (Moudi et al. 2007; Nkouathio et al. 2008; Gaele Nana et al. 2021). The CVL extends across the Gulf of Guinea from Pagalu, São

Tomé, Principe, and Bioko islands through Cameroon (Mts. Cameroon, Manengouba, Bambouto, Oku, Adamawa Plateau) to Lake Chad (Njome and De Wit 2014). The main feature within the CVL is Mount Cameroon which has remained active since the end of the Miocene and is located in the north-western part of the Kopongo area.

The CCSZ (Ngako et al. 2003) or fracture zone of Pernambuco-Tiko-Adamawa (Cornacchia and Dars 1983) is a ductile fault zone striking N70°E in Cameroon. It extends from the Trans-Brazilian Lineament to Sudan. The zone was rejuvenated several times, usually with a dextral movement, before and during the opening of the South Atlantic in the Cretaceous period (Dorbath et al. 1986). The CCSZ underlies a chain of CVL volcanoes which includes the active Mount Cameroon, Nyos and Monoun crater lakes, and several non-active ones. This shear zone is also considered a pre-drift extension of the Pernambuco fault in NE Brazil (De Almeida et al. 1981). During the late Pan-African tectonic evolution, the CCSZ was dextrally reactivated (Ngako et al. 1991). To the southeast of the studied area, the KCF trends almost in an N-S direction and may correspond to the northwestern margin of the Congo Craton. Reports from the Kribi area show that over sixteen earthquakes occurred in southern Cameroon during the last 100 years (Tabot et al. 1992; Nfoumou et al. 2004). Ateba et al. (1992) carried out several studies on seismic events and indicated that they are related to the volcanic activities of Mount Cameroon. The most recent earthquake in the region, with a magnitude of 3.2, occurred in July 2002 (Nfoumou et al. 2004). The southeastern part of the study area is bordered by the Sanaga fault which is a major crustal ductile deformation initially identified through remote sensing technique (Dumont 1986) and likely extends into the Central African Republic. This fault strikes N70°E and covers a distance of about 820 km along a fault axis zone of 100 km. This fault was reactivated during the Cretaceous (Ngako et al. 2008) and remains active till the present (Ndikum et al. 2014; Ngatchou et al. 2018; Moussango Ibohn et al. 2018).

Granulite and eclogitic facies assemblages, associated with charnockitisation and/or migmatization, have served as indicators to attest the Eburnean-Transamazonian geodynamic processes along the western margin of the Archean Congo craton dated at 2.1–2.0 Ga (Ledru et al. 1994; Teixeira and Figueiredo 1991; Penaye et al. 2004; Lerouge et al. 2006; Van Schmus et al. 2008; Weber et al. 2016; Loose and Schenk 2018; Bouyo Houketchang et al. 2019). In contrast, the presence of similar gneissic facies within the Eburnean and Pan-African belts has been highlighted as a Neoproterozoic rejuvenation dated at  $566 \pm 35$  (Toteu et al. 1994). The geological evolution of this group indicates of mafic-to-ultramafic facies in the form of orthogneisses, meta-quartzites pyroxenites, and amphibolites (Lerouge et al. 2006; Ebah Abeng et al. 2012; Chombong and Suh 2013), whereas the syn- to late-tectonic

orthopyroxene-garnet gneisses, alkaline syenites, and post-tectonic meta-diorites were considered main plutonic rocks (Toteu et al. 1994; Lerouge et al. 2006). More recently, Maurizot et al. (1986), Loose and Schenk (2018), and Bouyo Houketchang et al. (2019) identified several types of eclogitic facies and garnetiferous outcrops enclosed by micaceous quartzite, amphibolite, and gneiss/granulite country rocks in the NyG (Fig. 3).

Structurally, the NyG has been affected by  $D_n$ ,  $D_{n+1}$ ,  $D_{n+2}$  (Feybesse et al. 1998; Toteu et al. 1994; Abou'ou Ango et al. 2021, 2022), and  $D_{n+3}$  (Owona 2008; Abou'ou Ango et al. 2022) polyphase deformations.  $D_n$  corresponds to the first increments of crustal thickening, characterized by  $S_n$  relict foliation mostly concentrated on the  $F_{n+onefold}$  hinge zones and in paragenesis (Feybesse et al. 1998; Penaye et al. 2004). The  $D_{n+1}$  emplaced  $S_{n+1}$  flat-laying,  $F_{n+1}$  folds, and blastomylonitic  $C_{n+1}$  shear zones (Feybesse et al. 1998; Abou'ou Ango et al. 2022), whereas  $S_{n+2}$  mylonitic foliation,  $C_{n+2}$  shear planes,  $A_{n+twofold}$  axes, and  $F_{n+2}$  open folds represented the  $D_{n+2}$  geological structures (Feybesse et al. 1998; Abou'ou Ango et al. 2021, 2022). Meanwhile,  $F_{n+2}$  open folds constitute the structural scale forming the Nyong nappe transported top to East onto the Ntem Group, which were later dissected by sinistral NE-SW blastomylonitic shear zones (Feybesse et al. 1998; Minyem 1994; Penaye et al. 2004).  $D_{n+3}$  is documented by E-W, NE-SW, NNE-SSW, and ENE-WSW tension gashes, tension fractures, and faults (Owona 2008; Abou'ou Ango et al. 2022). This suggests that the Nyong Group discriminates against four tectonic events (Toteu et al. 1994; Ndema Mbongue et al. 2014; Abou'ou Ango et al. 2022).

### Geomorphological and climatic settings

Geographically, the study area lies between longitudes 10°06'E and 10°19'E and latitudes 03°53'N and 04°05'N. This area is considered to be located within Edea 2, Ngwei, and Dibamba districts of the Sanaga-Maritime sub-division of Edea town, Cameroon (Fig. 1c). The shape of the Kopongo area is slightly rectangular and comprises 518.6 km<sup>2</sup> area and 91.134 km of the perimeter, with the elevations range from 51.1 to 601 m. This region falls within a dense forest and tropical climate. Kopongo area belongs to the Sanaga watershed and west to south Cameroon Low Plateau (Ségalen 1967). The topographic variation of this area has been previously subdivided into three altitudes known as (1) lower altitudes ( $51.1 \leq LA \leq 169$  m), (2) intermediate altitudes ( $169 < IA \leq 305$  m), and (3) upper altitudes ( $305 < UA \leq 601$  m) (Fig. 3, Abou'ou Ango et al. 2021). Central Africa and Cameroon are summits of the same equatorial climate since the Miocene (Bamford 2000). The rises of planetary topography from the late Cretaceous to early Tertiary African and the late Tertiary post-Pan-African surfaces



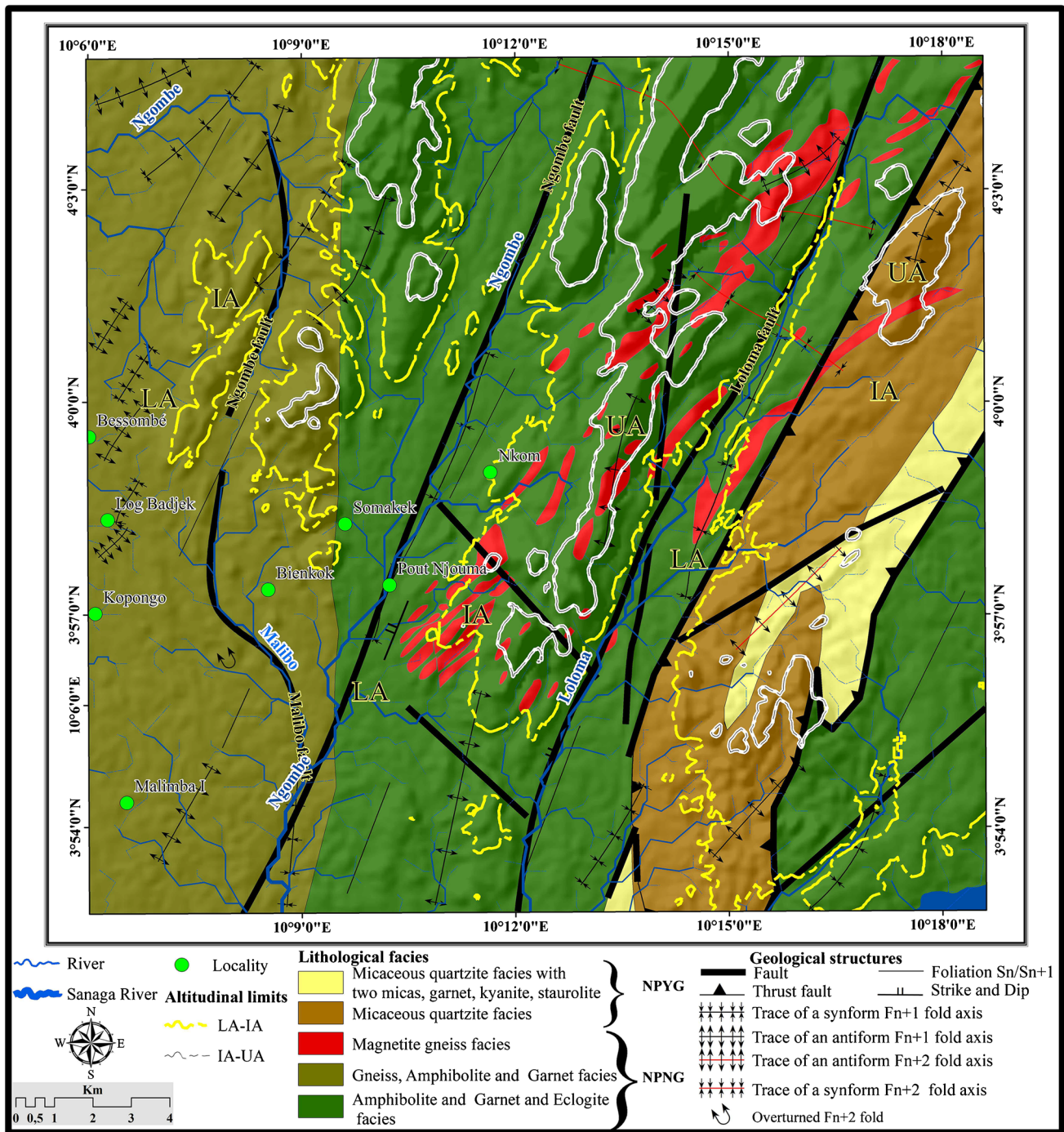


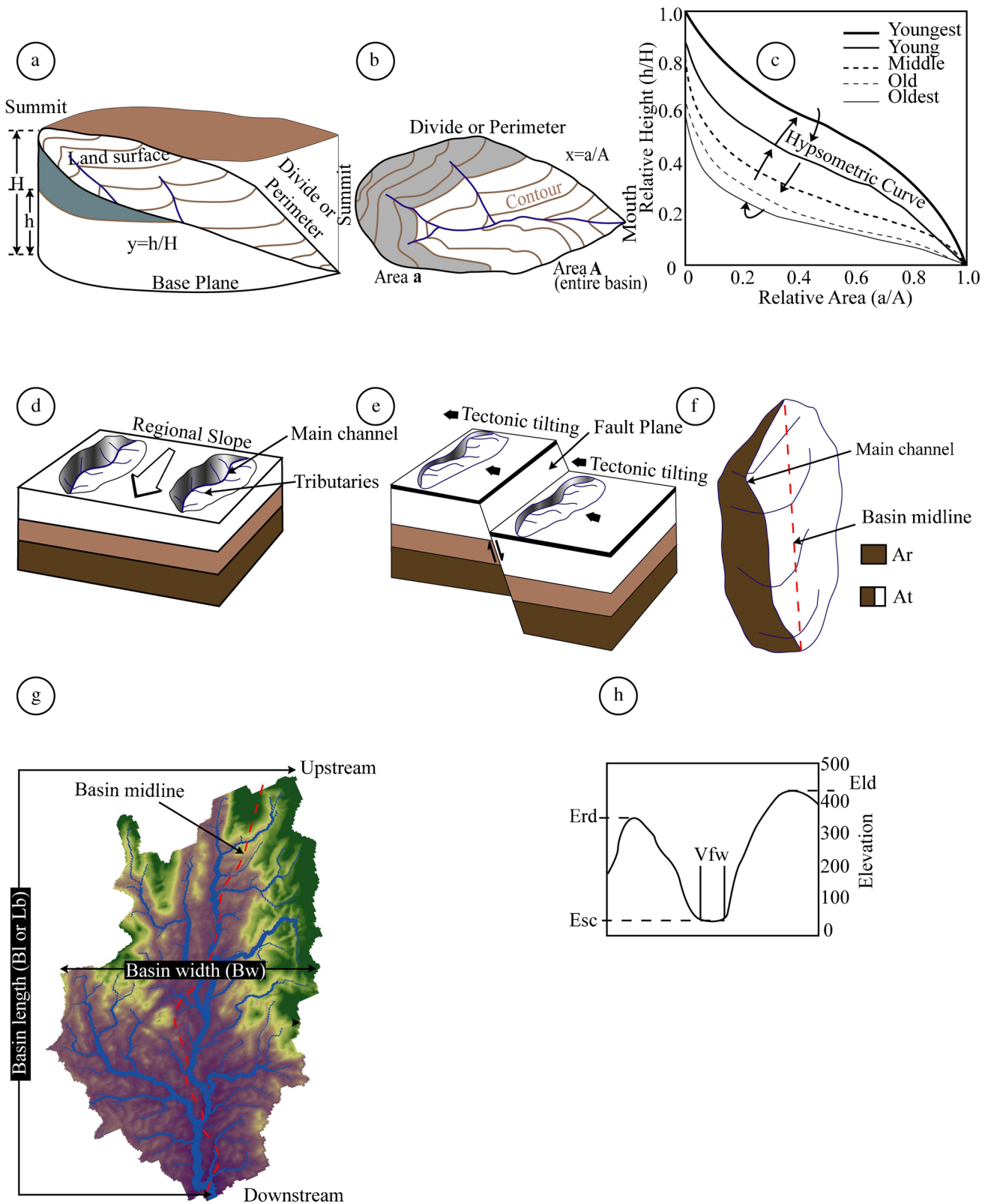
Fig. 3 Kopongo geological map extracted from Maurizot et al. (1986). This map was overlaid by the drainage network types

are all influenced by climatic variations (Nsangou Ngapna et al. 2020). Since the beginning of the Miocene, the whole region was affected by an equatorial Guinean climate with a pluviometry exceeding 4000 mm/yr (Ndam Ngoupayou et al. 2007; Regard et al. 2016). This climate contributes partially to landscape development and influences meteoric erosion (Nsangou Ngapna et al. 2020).

### Methodology

#### Source, acquisition, and data processing

The approach adopted for this study involves the use of SRTM (Shuttle Radar Topographic Mission) organized within a GIS environment. This DTM (Digital Terrain Model) radar image



was acquired from public source data, distributed freely by the United States Geological Survey (USGS, <https://earthexplorer.usgs.gov/>). This image was pit/depression filled using

ArcGIS environment on hydrology generic tools to avoid errors, remove voids, and resampled using bilinear interpolation techniques (e.g., Grohmann 2004; Abou'ou Ango et al.



**Fig. 4** Geomorphic indices parameters: **a–c** Top and plan views of hypsometric parameters with their different hypsometric curve models (modified after Strahler 1952). **d** Geometrical illustration of the main river channel without tectonic deformation influence. **e** Geometric representation of a river basin having undergone a modified tectonic deformation of the normal faults, modifying the flow channel. **f** Different parameters of AF are represented by the area of the basin to the right of the main channel (Ar) oriented downstream and the total area of the basin (At) (modified after Mahmood and Gloaguen 2012). **g** View in three dimensions of the Basin shape (Bs) associated with the contours, drainage divide, basin length (Bl), and basin width (Bl); **h** parameters of Vf viewed in two planes

2021). The resultant images were used in the calculation and extraction of the geomorphic indices and increasing the necessary vector layers such as elevation, sub-watersheds, drainage network, contour lines, and slope.

Sub-catchments of about twenty were generated and investigated with their parameters (Fig. 4) to calculate different morphometric indices such as hypsometric integral (Hi), hypsometric curve (Hc), asymmetry factor (AF), bifurcation ratio (Rb), basin shape ratio (Bs), relative tectonic uplift (U), and valley floor width to valley height ratio (Vf) (Tables 1 and 2) followed by the production of their respective maps. In the end, the relative active tectonic (IAT) values and map were obtained by a combination of all used indices (Table 2). Meanwhile, the drainage network classification was identified according to Strahler (1957). In parallel, ArcGis.10.8 extension known as “DEM Surface Tools©, Version 2.1.375” (Jenness 2013) was used to provide a slope inclination map using the classification proposed by Klimaszewski (1978).

Swath profile forms have been used to condense spatial information of the topographic patterns, river profiles, and geological structures (e.g., Pérez-Peña et al. 2016; Abou’ou Ango et al. 2021). In this study, the drainage patterns were investigated using the swath profiles function in MATLAB platform. A rectangular swath width of 2 km was chosen to extract a series of parallel profiles. On one hand, this width is large enough to appropriately condense both elevated surfaces and streams. On the other hand, it is small enough to avoid averaging topographic structures which are too oblique to the axis of the rectangular swath. Thus, in a GIS environment, statistical parameters such as maximum, minimum, and mean elevations were calculated along each swath profile. This method helped to provide longitudinal topographic stream profiles from obtained drainage network vector data to determine the incision zones.

## Fieldwork

Drainage catchments are sensitive to variations in tectonic intensity and their geometric characteristics depend on the combined action of tectonic forces and degradation processes. The shapes and patterns thus created can be studied

and analyzed qualitatively and quantitatively (Keller and Pinter 2002). Due to the immensity of the study area (500 km<sup>2</sup>), the simplified geological map by Maurizot et al (1986), with, 30 m resolution DTMs and a digitized topographic map (1: 200,000) were used as a guide and allowed the selection of specific sites for the field study. Based on these data, the fieldwork consisted of an identification of the morphological, structural and lithological types, and the geological changes. In addition, the detection of anomalies in the flow trajectories provides valid data for the development of geological structures that are used in approving the morphometric and morphotectonic interpretations made from the numerical values of the calculated geomorphic indices. During this fieldwork, several characteristics in terms of geological structures and contacts were observed and analyzed.

## Results

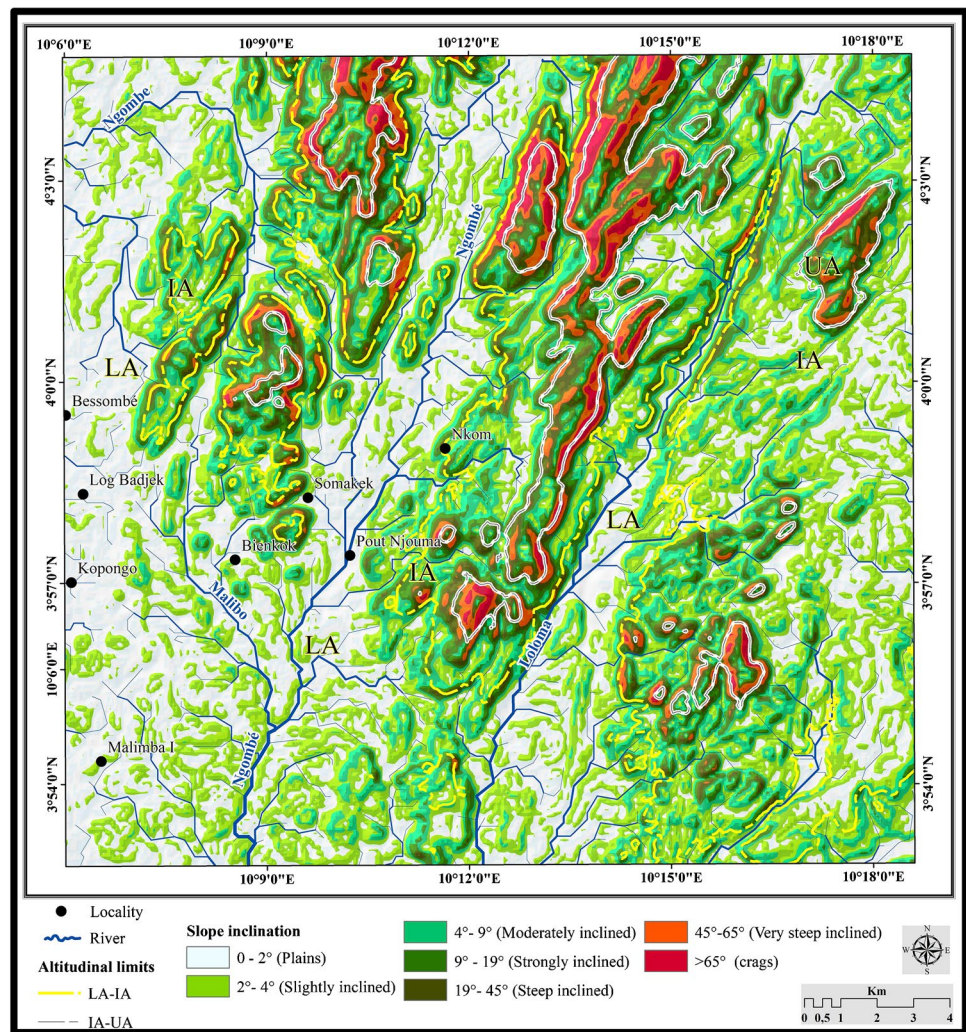
### Slope inclination

The slope map of the investigated area was classified into seven categories (Fig. 5): plains (0–2°), slightly inclined (2–4°), moderately inclined (4–9°), strongly inclined (9–19°), steep inclined (19–45°), very steep inclined (45–65°), and crags (> 65°). Plains and slightly inclined slopes occur all over the research area and are mainly associated with the hinge of synforms and flood valleys, but are more visible at the wide valley floors occupied by Loloma, Ngombé, and Malibo Rivers. Moderately, strongly, and steeply inclined slopes are mostly observed in the IA and are associated with escarpments, steep fold limbs, and structural hills. Very steep inclined and crags are more displayed by UA and are related to the highest ridges, very steep flank of the hill, very steep fold limbs, and hinge of antiforms.

### Drainage patterns

The present Kopongo river system shows a hierarchical and typological heterogeneity. Hydrographic network is marked by sub-parallel, sub-dendritic, curved trellis, contorted, angular, and colinear patterns (Fig. 6), whereas stream orders vary between 1 and 5 orders: Ngombe (5th order), Loloma (4th order), Malibo (3rd order), and their tributaries (1st to 2nd orders). The drainage patterns and lithology of this area are very complex and are influenced by geological structures including N-S, NW–SE, and NE-SW faults, and N-S, NE-SW, and NNE-SSW thrust faults and folds (Fig. 3). The presence of these geological structures controlled by

**Fig. 5** Kopongo slope inclination map



NNE-SSW topography translates slope variability from slightly inclined to crags (Fig. 5).

### Landform patterns

The Kopongo area displays a complex topography characterized by alternating flat to crag landscapes, developed within remobilized Archean Congo craton into Paleoproterozoic Nyong and Neoproterozoic Yaounde Groups (PPNG and NPYG, respectively), later covered by Cretaceous to recent Logbadjeck sediments. Three districts are highlighted in this area according to their elevation, slope, uplift variations, and lateral tilting (Fig. 3).

The LA includes Paleoproterozoic, Neoproterozoic, and sedimentary formations. It is crosscut and incised by Loloma, Ngombé, and Malibo Rivers and their tributaries (Fig. 3). It is also characterized by extensive slightly steep slopes, plains, and low relief all over the investigated area. The IA encompasses the entire moderate to steep slopes, and residual reliefs incised by 1st and 2nd order streams.

This altitudinal unit shows moderate to narrow V-shaped valleys occupied by resistant rock types (Fig. 3). The UA is crosscut and incised by the lower order stream (1st order). This geomorphic unit is characterized by the highest relief, low incision, very steep inclined slopes, crags, and narrow valleys that could correspond to the highest uplift rates and lateral tiltings. This is common in the central, northwest, northeast, and southeast parts overlaid by metamorphic rocks (Fig. 3).

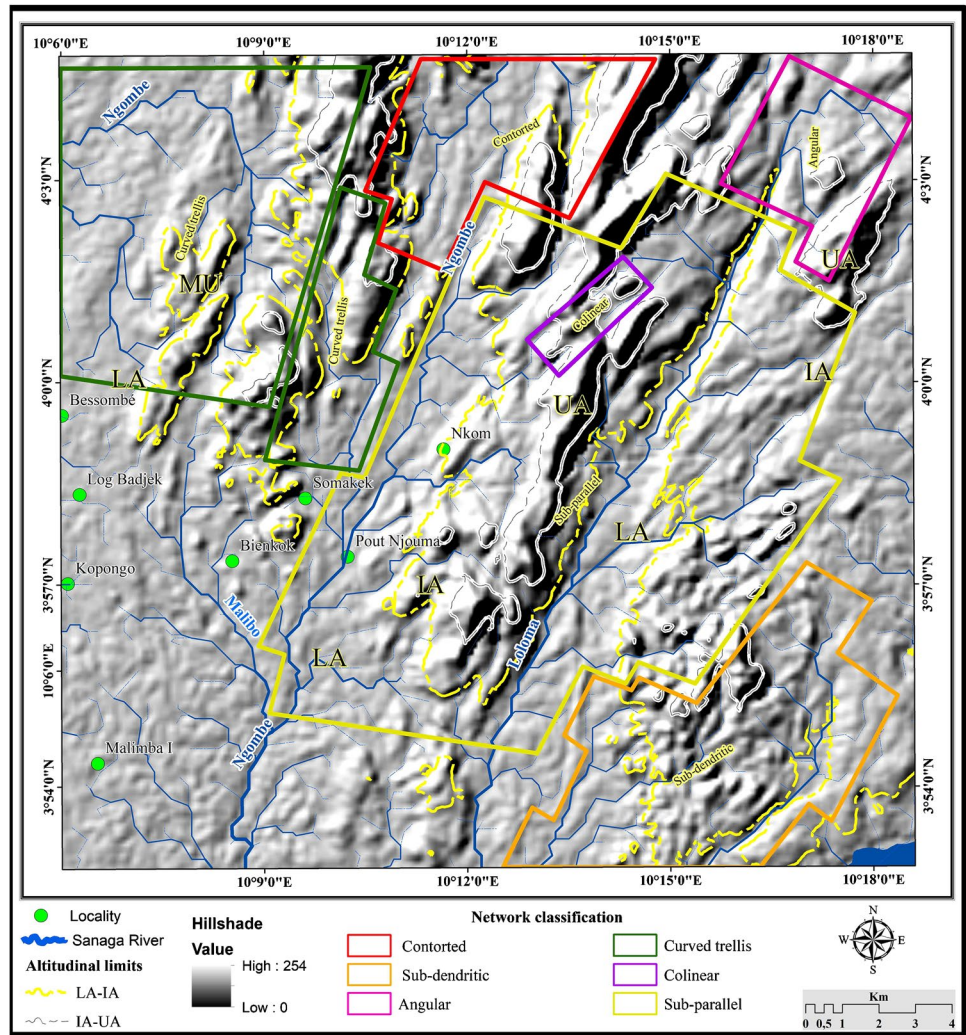
This indicates that the sedimentation zones are observed at the low altitudes, while the areas of strong erosion are located at the high altitudes.

### Field observations

This comprises samples obtained from outcrop and drill-core, and the different morphological changes produced by vertical uplift and tilting affecting the drainage pattern and landscape are all recorded (Figs. 7 and 8). It appears that the drainage system is controlled by geological structures



**Fig. 6** Drainage pattern classification map of the Kopongo area



inducing the river diversion (Fig. 7a) and channel incision (Fig. 8c). Paradoxically, there are some cases which show that the streamflow follows the direction parallel to the Ngombe strike-slip fault (Fig. 8c), perpendicularly to the fault plane (Fig. 8d) or parallel to the foliation (Fig. 7f). Besides, the river deviation and parallel flow do not show a close relationship with lithological heterogeneity, but can be related to a normal dip-slip fault (Fig. 7e and g), inverse dip-slip fault (Fig. 7g), and strike-slip faults with reverse and normal component (Figs. 7b and 8c, respectively). In addition, tectonic forces impose a topographic configuration that influences the flow of the hydrographic network.

From the structural point of view, Kopongo hills display a chocolate-slab pattern of blocks with intermontane depressions, bounded by detachment faults in an extensional environment (Fig. 8b). Besides, en echelon patterns of normal dip-slip faults are also observed along the corridor controlled by Ngombe River (Fig. 8e and f). Observations were made at the outcrop scale as well as on drillcore samples en echelon normal (Fig. 8d) and reverse (Fig. 7g) faults.

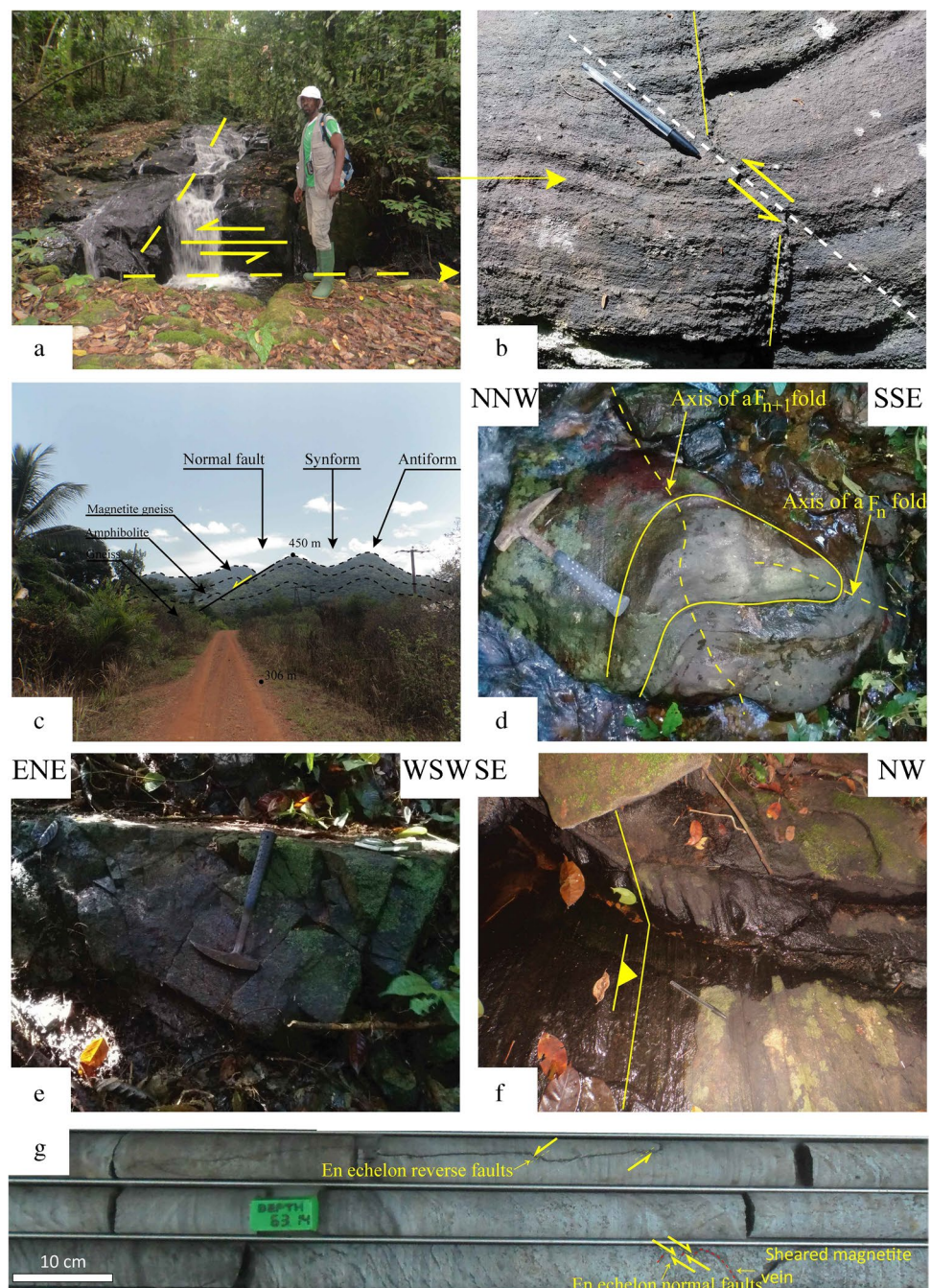
Because of the intensity of the pressures generated by tectonic stresses in the Kopongo region, the shear zones, tension gashes (Fig. 7b), and tension fractures (Fig. 7e) have been produced, especially over the metamorphic rocks. Consequently, the morphostructural pattern at the Kopongo is mainly characterized by asymmetric hills and plains. This suggests an alternating NNE-SSW trending asymmetrical antiforms and synforms at the regional scale crosscut by normal fault (Fig. 7e) and attested at the outcrop scale by two generations of the fold (Fig. 7d).

### Longitudinal profile analysis

The investigations carried out on the longitudinal profiles of the Loloma, Ngombé, and Malibo rivers (Fig. 9a–c), developed over a total cumulative length of 60 km, have enabled the general overview of the altitudinal behavior and list of the multiple incisions along these rivers. Moreover, these longitudinal profiles were elaborated on: (1) a 28 km long section of the Loloma river with elevations ranging



**Fig. 7** Field photo of geological structures of the Kpongong area: **a** river diversion. **b** Strike-slip fault. **c** Alternating antiform and synform crossed-cut par a normal fault. **d**  $F_n$  fold overprinted by  $F_{n+1}$  fold. **e** Network fractures. **f** The watercourse flows perpendicularly to the foliation. **g** En echelon normal and inverse dip-slip faults



from 95 to 239 m; (2) a 22 km long section of the Ngombe river, from 63 to 113 m; and (3) a 10 km long section of the Malibo river with a gradually increasing level of elevation from 73 to 110 m. Along some of the profiles (Fig. 9b and c), the elevation changes abruptly, whereas others (Fig. 9a) show gradual elevation, with localized abrupt changes. It is also observed that some maximum incisions along these main rivers ranged between 9 and 13 m. Loloma topographic profile shows a maximum incision of up to 13 m, while Ngombe and Malibo rivers displayed their respective incisions of 9 and 10 m. This suggests that zones within the

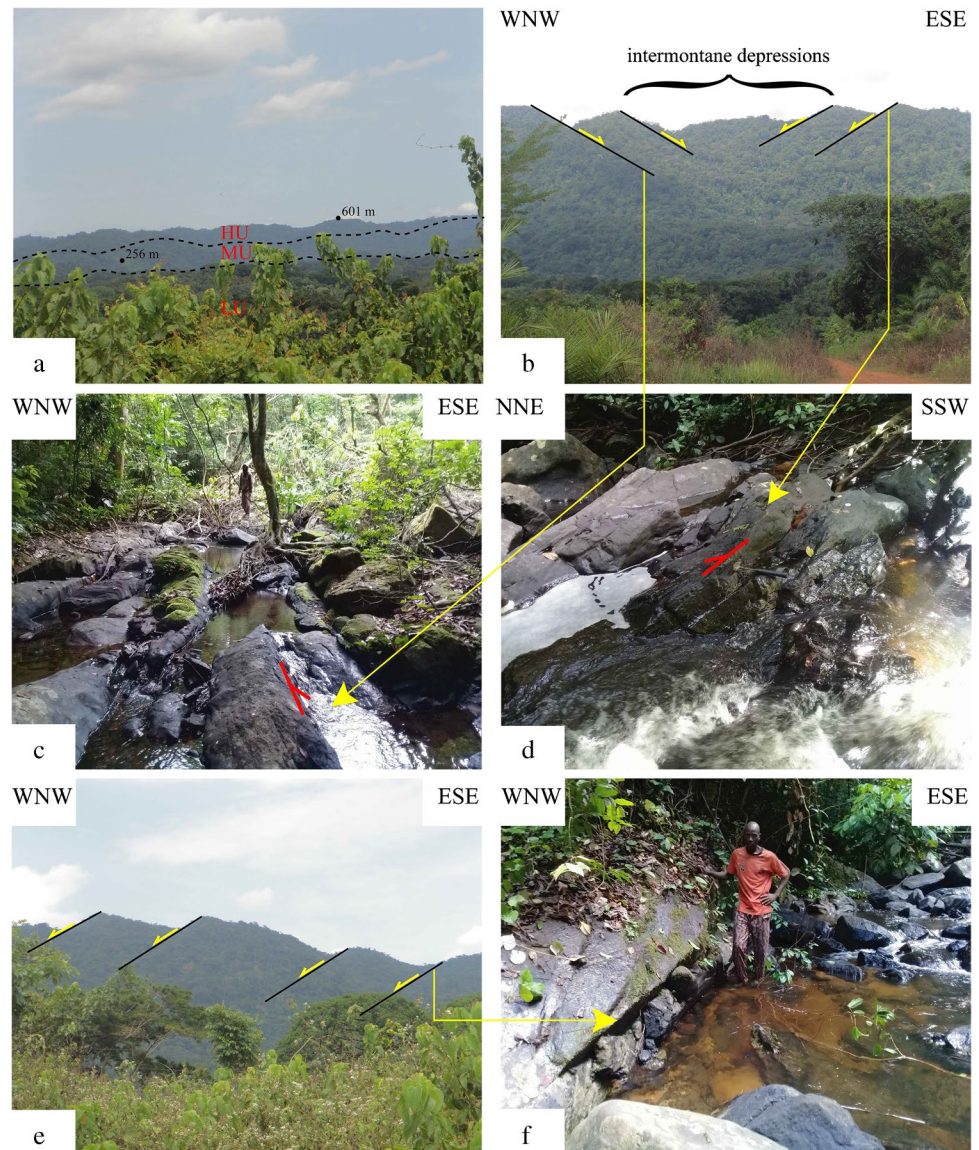
investigated area with significant incisions are tectonically active. Indeed, the different incisions observed characterize vertical to oblique slips produced by brittle geological structures or unequal distribution of tectonic forces inducing these deformations.

### Tectono-geomorphic responses

Hi-values are assigned and grouped into two classes: 2 and 3, varying between 0.12 and 0.51 (Table 3; Fig. 10). Class 2 (~ 16.63%; 76.75 km<sup>2</sup>) and class 3 (~ 83.39%; 384.78



**Fig. 8** Kopongo geological structures: **a** morphological units. **b** Kopongo hills display a chocolate-slab pattern of blocks with intermontane depressions, bounded by detachment faults in an extensional environment. **c** Ngombe channel incision with the watercourse flowing along the Ngombestrike-slip fault or in parallel. **d** Watercourse flowing perpendicularly to the normal dip-slip fault. **e** En echelon normal dip-slip faults. **f** Normal dip-slip fault



$\text{km}^2$ ) correspond to moderate and low tectonic activities, respectively (Table 3; Fig. 10). This variability of the  $H_i$ -values suggests a difference of the maturity of sub-basins. The hypsometric curves obtained from these sub-basins are divided into three different shapes, with concave (less mature), S-shaped (mature), and complex hypsometric curves (Fig. 10). The results indicated in Table 5 show that 15.11–20.79% of the  $H_i$ -values, with the basin area which gradually decreases from LA (76.75  $\text{km}^2$ ) to UA (4.96  $\text{km}^2$ ), are displayed by class 2, while class 3 consists of the higher values (~79.21–84.89%) and their areas > 27.87  $\text{km}^2$ . From this observation, evidence of tectonic activities of ~43.47% (200.66  $\text{km}^2$ ; LA), ~50.88% (234.84  $\text{km}^2$ ; IA), and ~5.65% (32.83  $\text{km}^2$ ; UA) is observed over the investigated area (Table 6).

The values of  $U$  vary from 0.16 to 0.68 and were categorized into three different classes (Table 3; Fig. 11a). These different responses to tectonic uplift, unequivocally point towards the landscape anomalies. Three classes are identified: 1 (~2.66%; 12.28  $\text{km}^2$ ), 2 (~42.40%; 195.69  $\text{km}^2$ ), and 3 (~54.95%; 253.62  $\text{km}^2$ ) and typified as high, moderate, and low (mild subsidence) active tectonics, respectively (Fig. 11a). In the present study, as depicted in Table 5, class 1 shows their lower values in the IA (3.93%, 7.22  $\text{km}^2$ ) and UA (11.45%, 5.06  $\text{km}^2$ ); class 2 displays their low to moderate values in the LA (~7.41%, 17.31  $\text{km}^2$ ), IA (~78.53%, 144.19  $\text{km}^2$ ), and UA (~77.29%, 34.16  $\text{km}^2$ ), whereas class 3 exhibits their decrease values from LA (~92.59%, 216.37  $\text{km}^2$ ) to UA (~11.27%, 4.98  $\text{km}^2$ ). Thus, this reaffirms an influence of uplift or subsidence of ~50.64% (233.73  $\text{km}^2$ ;

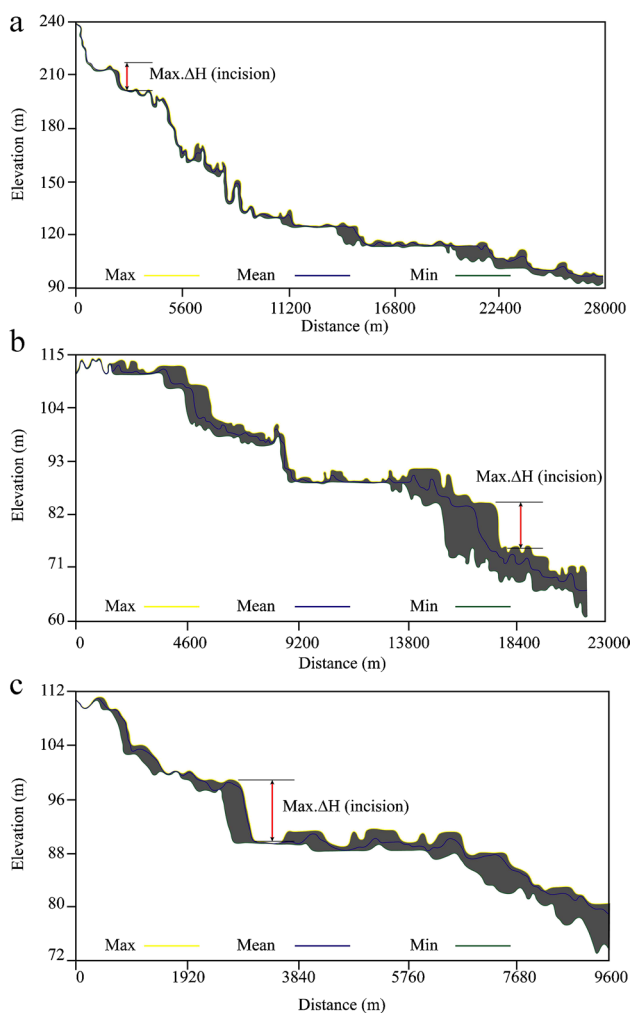


**Fig. 9** Topographic swath profiles elaborated across the Loloma (a), Ngombe (b), and Malibo (c) main rivers (see map in Fig. 1d)

LA), ~39.78% (183.61 km<sup>2</sup>; IA), and ~9.58% (44.20 km<sup>2</sup>; UA) (Table 6).

Table 3 and Fig. 11b show that Bs ranges in values from 1.13 to 3.02 and defines three classes: 1 (90.05%; 415.62 km<sup>2</sup>), 2 (8.63%; 39.83 km<sup>2</sup>), and 3 (1.33%; 6.09 km<sup>2</sup>). Class 1 (elongated sub-basin), class 2 (elongated to sub-elongated sub-basin), and class 3 (more circular sub-basin) are related to high, semi-, and low tectonic activities, respectively (Fig. 11b). Moreover, Table 5 indicates that Bs-values with their respective basin areas decrease from LA (~90.24%; 230.9 km<sup>2</sup>) to UA (~89.79; 35.81 km<sup>2</sup>) in class 1, while classes 2 (8.48%; 4.07–21.71 km<sup>2</sup>) and 3 (1.27%; 2.84–3.25 km<sup>2</sup>) illustrate their irregular lower values from one unit to another. Thus, drainage sub-basins belonging to class 1 have a longitudinal and narrow geometry revealing a rapid uplift, while class 2 tends to evolve by a progressive uplift rate. The above inhomogeneity of Bs-values exhibits a spatial variability of uplift

rate of ~55.44% (255.86 km<sup>2</sup>; LA), ~35.92% (165.80 km<sup>2</sup>; IA), and ~8.64% (39.88 km<sup>2</sup>; UA) over the entire explored site (Table 6).

Values of the IAF-50I indices over the study area ranging between 0.06 and 35.6 and four classes can be obtained (Table 4; Fig. 12). Class 1 (14.92%; 68.86 km<sup>2</sup>) shows strongly asymmetric sub-basins with intense tectonic activity, causing high tilting to the NE (e.g., SW-III). Class 2 (6.70%; 30.92 km<sup>2</sup>) implies moderately asymmetric sub-basins associated with high tectonic activity, and class 3 (43.22%; 199.48 km<sup>2</sup>) indicates gently asymmetric sub-basins with semi-tectonic activity, whereas class 4 (35.17%; 162.32 km<sup>2</sup>) belongs to symmetric sub-basins reflecting low tectonic activity associated with tilting to the SE-NW and suggesting an equilibrium state (e.g., SW-VI). From LA to UA, AF index anomalies recorded by classes 1 (~16.45–5.65%; 36.98–3.65 km<sup>2</sup>), 3 (~61.52–38.15%; 94.33–39.72 km<sup>2</sup>), and 4 (~42.46–30.76%; 72.8–20.14 km<sup>2</sup>) are disturbed, with basin area gradually decreasing, while class 2 (~11.01–1.63%; 24.84–1.05 km<sup>2</sup>) generally shows their decrease values (Table 5). This confirms ~48.86% (225.52 km<sup>2</sup>; LA), ~37.15% (171.46 km<sup>2</sup>; IA), and ~13.99% (64.56 km<sup>2</sup>; UA) of tilted surfaces all over the Kopongo area (Table 6).

The values and classes of Rb (bifurcation ratio) and Rbm (mean bifurcation ratio) are given in Table 4 and Fig. 13a. The Rbm ranges from 1.20 to 5.88. Three classes of Rbm are summarized: 1 (~33.07%; 152.63 km<sup>2</sup>), 2 (~45.88%; 225.60 km<sup>2</sup>), and 3 (~18.06%; 83.31 km<sup>2</sup>) that correspond to high, moderate, and low tectonic activities, respectively. Besides, they display their irregular values from LA to UA (Table 5): 1 (~25.14–44.60%; 13.49–70.77 km<sup>2</sup>), 2 (~20.49–57.88%; 6.34–157.42 km<sup>2</sup>), and 3 (~35.91–16.41%; 11.11–46.16 km<sup>2</sup>). Thus, Table 6 reflects a tectonic complexity of ~58.92% (271.95 km<sup>2</sup>; LA), ~34.38% (158.65 km<sup>2</sup>; IA), and ~6.70% (30.94 km<sup>2</sup>; UA) all over the landscape.

Vf-values varying from 0.17 to 1.92 were grouped into three classes (Table 4; Fig. 13b): 1 (15.38%; 70.98 km<sup>2</sup>), 2 (44.51%; 205.43 km<sup>2</sup>), and 3 (40.12%; 185.17 km<sup>2</sup>) that which indicate tectonically active regions with high, moderate, and low levels, respectively. All the Vf-values less than 0.48 revealed deeply incised and narrow V-shaped, and tight valleys. The intermediary values show irregular-shaped valleys, while the higher values of Vf are indicative of U-shaped valleys. From LA to UA, ~11.64–23.16% (11.49–32.48 km<sup>2</sup>) values of Vf were of class 1, ~25.94–54.59% (18.74–140.65 km<sup>2</sup>) were of class 2, and ~33.77–53.01% (19.37–86.99 km<sup>2</sup>) were of class 3 (Table 5). Indeed, unequal distribution of uplift and incision rates of 55.82% (257.64 km<sup>2</sup>; LA), 33.43% (154.30 km<sup>2</sup>; IA), and 10.75% (49.60 km<sup>2</sup>; UA) all over the area (Table 6).

**Table 3** Classification of the geomorphic indices

Sub-watersheds	Geomorphic indices					
	HI	HI_Class	U	U_Class	Bs	Bs_Class
I	0.32	3	0.34	2	2.80	1
II	0.23	3	0.26	3	1.99	1
III	0.32	3	0.27	3	2.34	1
IV	0.35	3	0.36	2	2.23	1
V	0.21	3	0.28	3	1.24	2
VI	0.32	3	0.34	2	1.80	1
VII	0.32	3	0.20	3	2.35	1
VIII	0.50	2	0.55	2	1.57	2
IX	0.50	2	0.57	2	2.07	1
X	0.50	2	0.68	1	3.02	1
XI	0.50	2	0.53	2	2.40	1
XII	0.50	2	0.26	3	2.04	1
XIII	0.51	2	0.16	3	1.79	1
XIV	0.50	2	0.25	3	1.41	2
XV	0.50	2	0.27	3	1.13	3
XVI	0.50	2	0.26	3	1.13	3
XVII	0.50	2	0.41	2	1.38	2
XVIII	0.50	2	0.46	2	2.07	1
XIX	0.51	2	0.41	2	1.85	1
XX	0.50	2	0.62	1	1.79	1

### Assessment of relative active tectonics (IAT)

The average values obtained from six classes of geomorphic indices including Hi, U, Bs, AF', Rb, and Vf (IAT) helped to classify the different studied sub-watersheds as a function of their IAT (Table 4; Fig. 14). Class 2 (14.89%; 68.72 km<sup>2</sup>), class 3 (72.71%; 335.58 km<sup>2</sup>), and class 4 (12.33%; 56.90 km<sup>2</sup>) are high, moderate, and low active tectonics, respectively. Then, from LA to UA, ~20.88–84.88% (14.47–169.43 km<sup>2</sup>) values of IAT were of class 2, ~25.27–37.70% (14.47–126.52 km<sup>2</sup>) were of class 3, and ~7.41–48.36% (4.22–39.74 km<sup>2</sup>) were of class 4 (Table 5). This shows that the region underwent various levels of tectonic activities from one unit to another with ~48.16% (222.31 km<sup>2</sup>; LA), ~35.11% (162.03 km<sup>2</sup>; IA), and ~16.72% (77.19 km<sup>2</sup>; UA) (Table 6).

## Discussion

### Geotectonic evolution of the Kopongo area through geomorphic indices

Based on the results of geomorphic, morphotectonic analysis, and extensive field campaigns, Kopongo site is considered to be a tectonically active zone, due to the presence of significant topographic and hydrographic anomalies.

Indeed, the intensity of the tectonic activities and the multiple indicators of the regional deformation within the area have been demonstrated through the field data and the values obtained from the geomorphic indices (e.g., Hi, Hc, U, AF, Rb, Bs, and Vf).

Hi and Hc values in the Kopongo area vary from one sub-watershed to another (Table 3; Fig. 10), and considerably from LA to UA (Tables 5 and 6). Following the classification proposed by Strahler (1952), this altitudinal variability is a major characteristic of less mature (LA) and mature (UA) sub-basins. In addition, the high, moderate, and low values of Hi coincide with the concave (less mature), S-shape (mature), and complex hypsometric curves, which allow the appreciation of fluctuations of the active tectonics detected for the Ngombe, Loloma, and Malibo major strike-slip faults (Fig. 3), coupled with the reactivation of old faults Sanaga (Ndikum et al. 2014; Noel et al. 2014; Moussango Ibohn et al. 2018; Nsangou Ngapna et al. 2020) and Kribi-Campo (Nfoumou et al. 2004; Sandron et al. 2018) faults close to the Kopongo area. Besides, concave, S-shape, and complex hypsometric curves obtained in this study show shape variabilities corroborating with the tectonic instabilities. The S-shape curves represent the moderately eroded region in which the topography evolves in the steady-state sub-basins (e.g., SWs-IV, VIII, and IX), while concave shape curves characterize highly eroded and fractured regions due



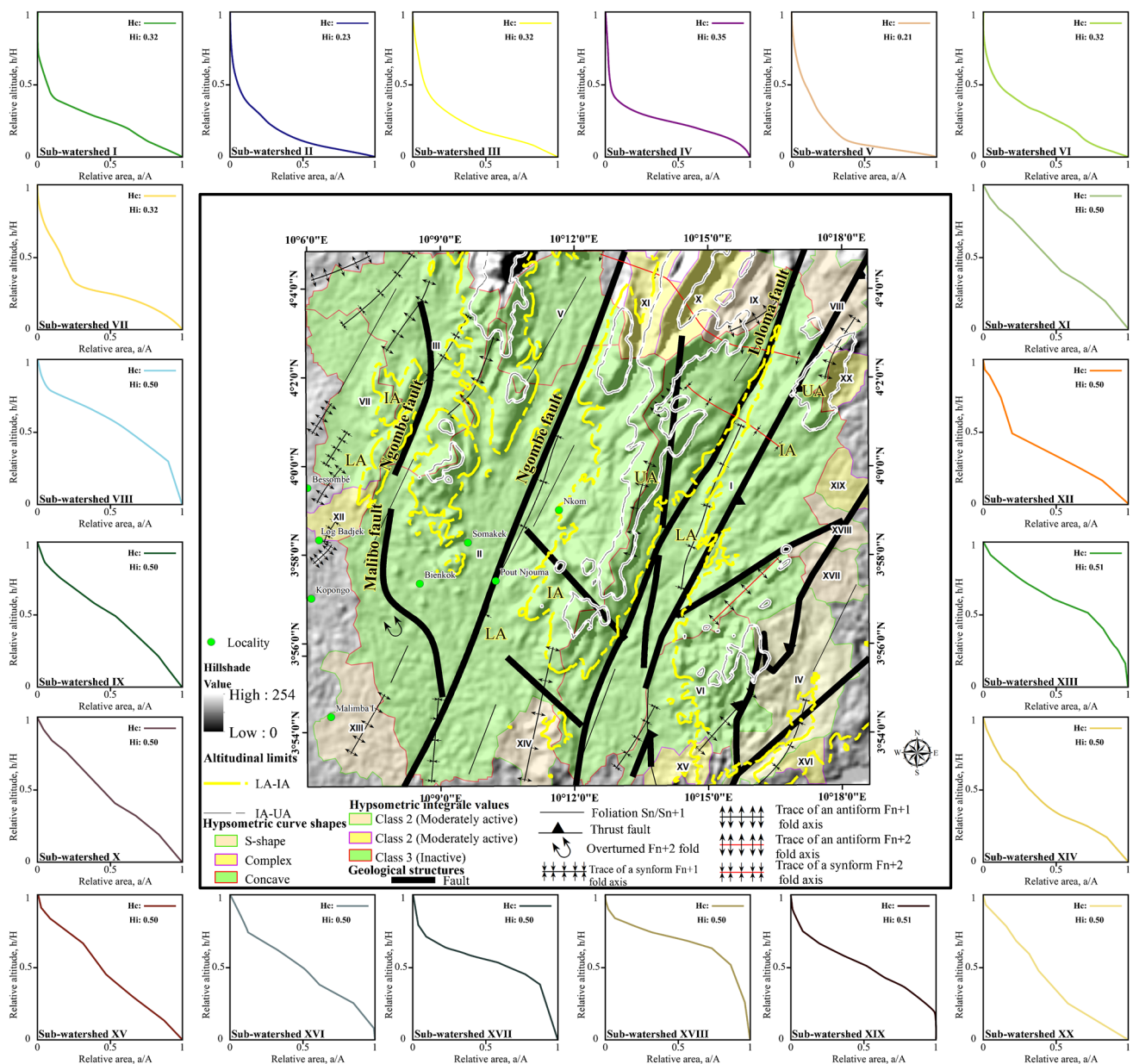


Fig. 10 Kopongo hypsometric parameters map

to structural discontinuities (e.g., SWs-X, XI, and XII, Pérez-Peña et al. 2009). On one hand, the spatial distribution from lower (0.21–0.35, LU) to higher (0.50–0.51, IA and UA)  $H_i$ -values shows that several kilometers of areas were characterized by remarkably high rates of denudation, whereas on the other hand, relatively significant rock masses have been eroded (El Hamdouni et al. 2008). Since the shape of the curve describes lateral erosion, the irregular shapes observed at the upstream and downstream (e.g., SWs-XIX and XX) could positively correlate to rejuvenation processes, piracy events, or differential uplift associated with strong heterogeneity of geological formations

(Fig. 3, Ajay Kumar et al. 2018). Differences observed in the  $H_i$  (Tables 5 and 6) and the  $H_c$  (Fig. 10) can be attributed to the uplift caused by neotectonic processes (e.g., Gu and Shi 2018). Thus, moderate ( $0.50 < H_i$ ) and high ( $0.50 < H_i < 0.7$ ) values of  $H_i$  obtained prove that the Kopongo area is influenced by weak (e.g., LA) and moderate (e.g., IA and UA) tectonic uplift activities indicative of a rejuvenation.

According to Kirby and Whipple (2012), the landscape and stream anomalies due to uplift rate processes testify to the type, time, and geometry of tectonic forces in the extensive and compressive environment. Consequently,



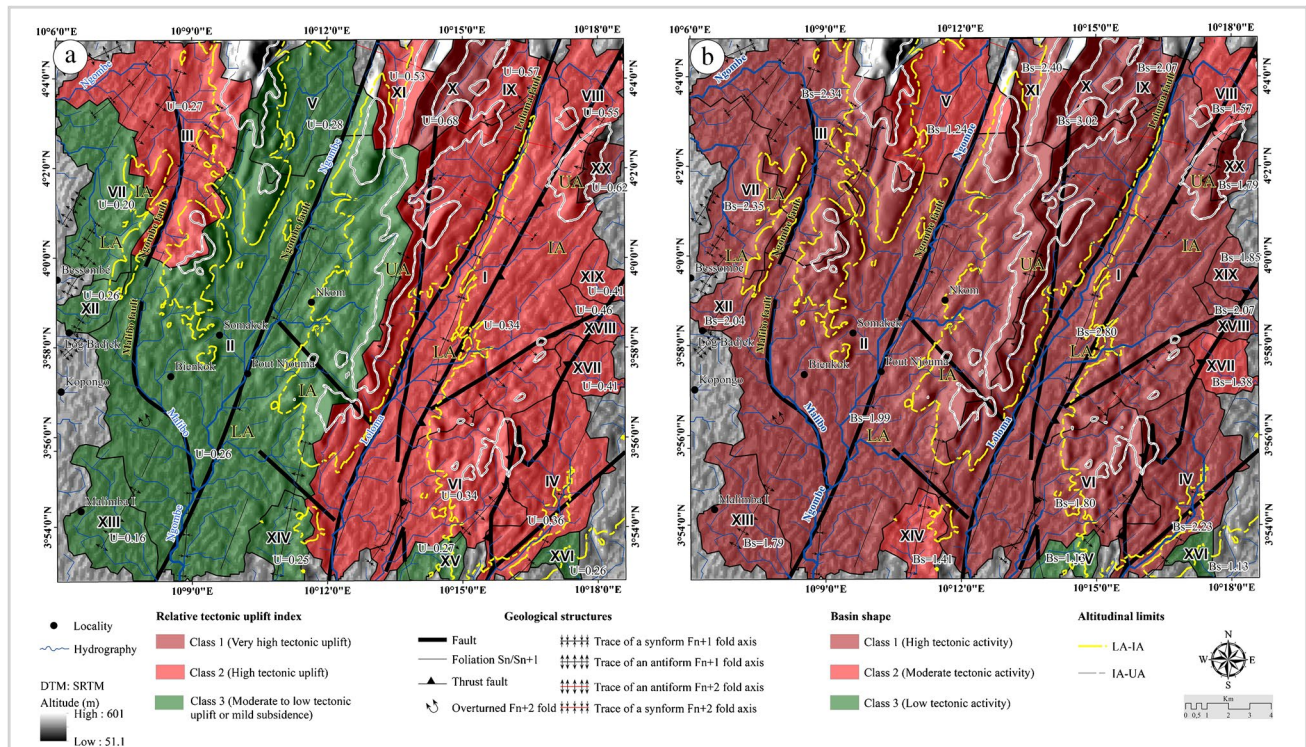
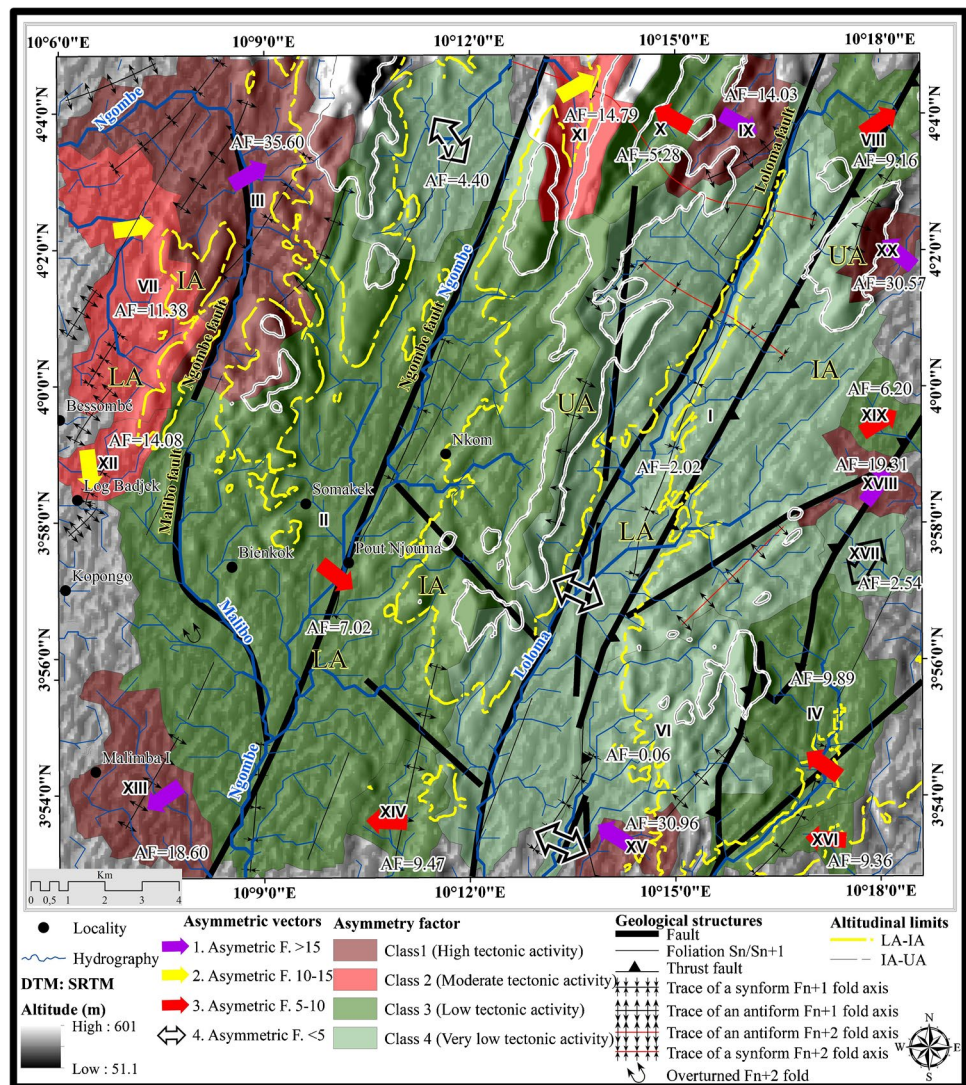


Fig. 11 Geomorphic indices maps: a index of relative tectonic uplift and b basin shape of the Kopongo area

Table 4 Classification of the geomorphic indices

Geomorphic indices										
Sub-watersheds	AF	AF'	AF'_Class	Rb	Rbm	Rbm_Class	Vf	Vf_Class	IAT	IAT_class
I	47.98	2.02	4	2.41–10.67	5.36	1	2.04	3	2.33	3
II	42.98	7.02	3	1.98–10.60	4.27	2	0.52	2	2.33	3
III	85.59	35.60	1	3.75–8.00	5.88	1	0.59	2	1.83	2
IV	59.89	9.89	3	4.00–4.50	4.25	2	0.48	1	2.00	3
V	54.40	4.40	4	3.75–4.00	3.88	2	1.00	3	2.83	4
VI	49.94	0.06	4	3.75–4.00	3.88	2	1.38	3	2.50	4
VII	61.38	11.38	2	2.50–3.00	2.75	3	0.41	1	2.17	3
VIII	59.16	9.16	3	1.50–2.33	1.92	3	0.21	1	2.17	3
IX	65.03	15.03	1	2.00	2.00	3	0.75	2	1.83	2
X	44.72	5.28	3	1.25	1.25	3	0.32	1	1.83	2
XI	64.79	14.79	2	1.67–3.00	2.33	3	0.17	1	1.83	2
XII	64.08	14.08	2	2.00	2.00	3	1.92	3	2.33	3
XIII	68.60	18.60	1	1.29–7.00	4.14	2	1.15	3	2.00	3
XIV	40.53	9.47	3	1.20	1.20	3	0.61	2	2.50	4
XV	19.04	30.96	1	1.33	1.33	3	0.45	1	2.17	3
XVI	40.64	9.36	3	2.00	2.00	3	1.03	3	2.83	4
XVII	47.46	2.54	4	1.25	1.25	3	1.05	3	2.67	4
XVIII	69.31	19.31	1	2.00	2.00	3	0.90	2	1.83	2
XIX	56.20	6.20	3	1.33	1.33	3	1.71	3	2.33	3
XX	19.43	30.57	1	2.00	2.00	3	0.69	2	1.67	2

**Fig. 12** Basin asymmetric factor map of the Kopongo area



climatic variations can be linked to tectonic uplift events (Dana 1856). In this case, either the climate change that took place at the end of the Cenozoic caused a direct or indirect tectonic uplift or the erosion rates associated with isostatic compensations during this climatic variation can not have definite resolutions in the face of the problem observed, to generate vertical motions (Hay et al. 2002). The available data in the African continent show significant climatic changes from the Cretaceous to the present (Burke and Gunnell 2008; Grimaud 2014; Mvondo Owono et al. 2022). It has also been reported that Africa registered a humid period during the Aquitanian early Miocene (Bamford 2000), while the SW coast became and remained arid after the middle Miocene (Pickford and Senut 1999). The same climatic evolution has been observed in southwestern Cameroon in the Rio Del Rey basin (Mvondo Owono et al. 2022) and Edea-Eseka region (Nsangou Ngapna et al. 2020) located within the Gulf of Guinea. The southwestern Cameroon

region has been submitted since the early Miocene to an equatorial typical Guinean climate. Kopongo falls within the same climate region and displays three main seasons: a short dry season (3 months), a short humid season (3 months), and a very long rainy season (6 months) (Sighomnou 2004). Within the investigated area, the pluviometry measured up to 3512 mm/yr (Tchindjang et al. 2015), with temperatures between 28 and 33 °C and a 70% of humidity rate (Olivry 1986). According to Mvondo Owono (2011), volcanism is another phenomenon that can affect the morphology of a region. Indeed, the Cenozoic intraplate volcanism that has affected the Gulf of Guinea appears as discrete centers or linear zones, associated with the domal uplift of the basement (Poudjom Djomani et al. 1995). The Cameroon Volcanic Line (CVL) that traverses the Gulf of Guinea has developed uplifts during the Tertiary. This activity became very prolific due to the activity of Mount Cameroon volcano, one of the most important and active volcanoes along the CVL found



**Table 5** Geomorphic indice values grouped in classes and morphological units with their respective frequency (Freq.%) and area (A, km<sup>2</sup>)

Geomorphic indices	Classes	Morphological units					
		LA		IA		UA	
		Freq	A	Freq	A	Freq	A
HI	2	~ 16.83	76.75	~ 20.79	48.82	~ 15.11	4.96
	3	~ 83.17	166.88	~ 79.21	186.02	~ 84.89	27.87
U	1			~ 3.93	7.22	~ 11.45	5.06
	2	~ 7.41	17.31	~ 78.53	144.19	~ 77.29	34.16
Bs	3	~ 92.59	216.37	~ 17.54	32.25	~ 11.27	4.98
	1	~ 90.24	230.9	~ 89.81	148.91	~ 89.79	35.81
	2	~ 8.48	21.71	~ 8.47	14.05	~ 10.21	4.07
AF'	3	~ 1.27	3.25	~ 1.71	2.84		
	1	~ 16.40	36.98	16.45	28.22	~ 5.65	3.65
	2	~ 11.01	24.84	~ 2.93	5.02	~ 1.63	1.05
Rbm	3	~ 41.82	94.33	~ 38.15	65.42	~ 61.52	39.72
	4	~ 30.76	69.37	~ 42.46	72.8	~ 31.20	20.14
	1	~ 25.14	68.37	~ 44.60	70.77	~ 43.60	13.49
	2	~ 57.88	157.42	~ 38.97	61.84	~ 20.49	6.34
Vf	3	~ 16.97	46.16	~ 16.41	26.04	~ 35.91	11.11
	1	~ 11.64	30	~ 21.05	32.48	~ 23.16	11.49
	2	~ 54.59	140.65	~ 25.94	40.03	~ 37.78	18.74
IAT	3	~ 33.77	86.99	~ 53.01	81.79	~ 39.06	19.37
	2	~ 20.88	14.47	~ 30.76	21.13	~ 48.36	33.23
	3	~ 50.45	169.43	~ 37.70	126.52	~ 11.84	39.74
	4	~ 84.88	38.41	~ 25.27	14.38	~ 7.41	4.22

**Table 6** Geomorphic indice values are grouped in morphological units with their respective frequency (Freq. %) and area (A, km<sup>2</sup>)

Geomorphic indices	Morphological units/districts					
	LA		IA		UA	
	Freq. (%)	A (km <sup>2</sup> )	Freq. (%)	A (km <sup>2</sup> )	Freq (%)	A (km <sup>2</sup> )
HI	~ 43.47	200.66	~ 50.88	234.84	~ 5.65	32.83
U	~ 50.64	233.73	~ 39.78	183.61	~ 9.58	44.2
Bs	~ 55.44	255.86	~ 35.92	165.8	~ 8.64	39.88
AF'	~ 48.86	225.52	~ 37.15	171.46	~ 13.99	64.56
Rbm	~ 58.92	271.95	~ 34.38	158.65	~ 6.70	30.94
Vf	~ 55.82	257.64	~ 33.43	154.3	~ 10.75	49.6
IAT	~ 48.16	222.31	~ 35.11	162.03	~ 16.72	77.19

in proximity to the study area. The mountain contributes to a very important uplift whose rate was evaluated at ~ 3.8 m/Ma by Koum et al. (2013). Given these conditions, the landscape of the Kopongo area has undergone rejuvenation and demonstrates a transient geomorphic response as feedback to tectonic-climatic forcing. Thus, the interplay among tectonic uplift, climate, erosion, and vegetation on the landscape evolution in a region has been indisputably documented, since the modification of one of the factor products for an immediate disequilibrium and changes. In Cameroon, these tectonic uplifts are marked by the presence of young geological

structures illustrated by the Benue trough and the basaltic ridge of the CVL which extends from the Atlantic Ocean to north Cameroon (Goussi Ngalamo et al. 2017). This tectonic consequence also shows that the thickness of the continental crust in Cameroon is thinned and varies between ~ 50 km in the south and ~ 14 km in the north. This suggests an important rise of the Moho towards the north of ~ 50–32 km under the Congo Craton, ~ 32–22 under the Adamawa plateau, and 22–18 km under the western portion of Cameroon (Fig. 15a, Poudjom Djomani et al. 1995). Kopongo area is close to the basaltic ridge of the CVL where the crustal thickness

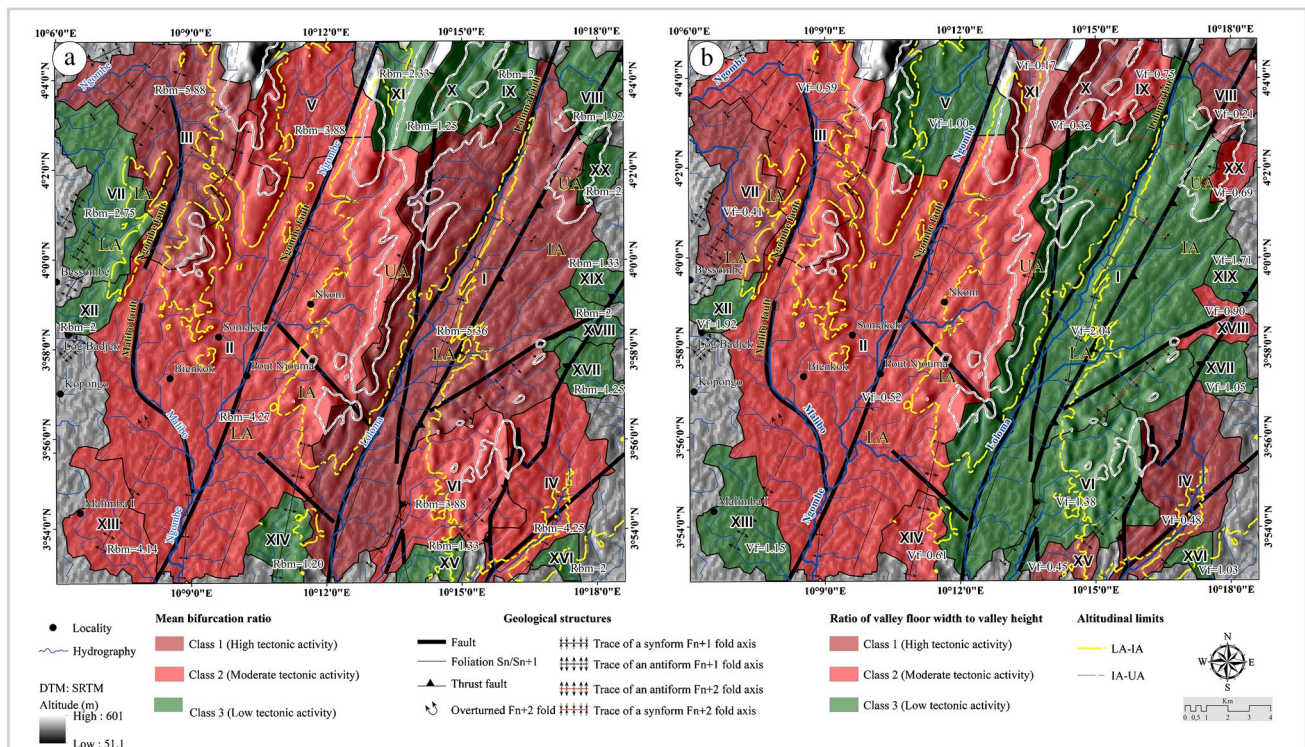


**Fig. 13** Maps of the Kopongo geomorphic indices: **a** bifurcation ratio and **b** valley floor width to valley height ratio

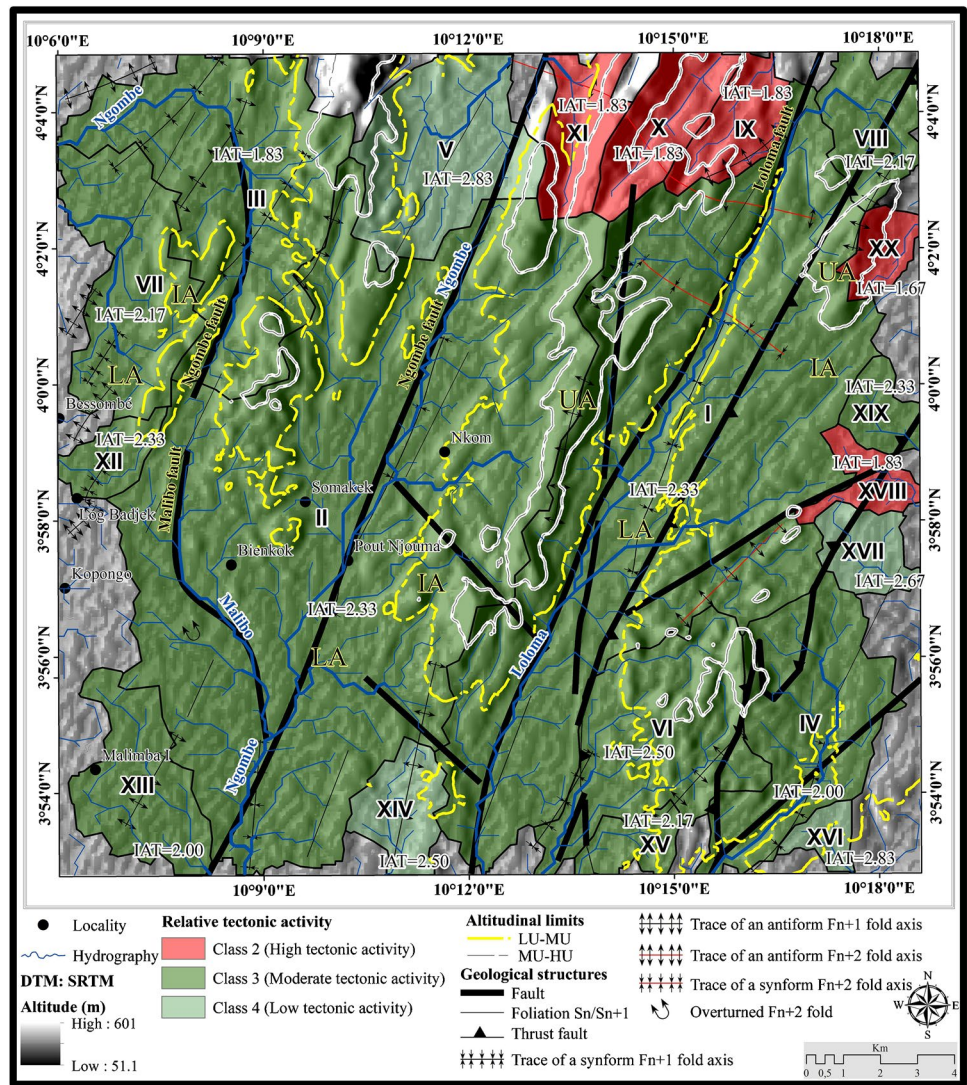
varies from 27 to 35 km (e.g., Noel et al. 2014). The tectonic uplift in Central Africa varies from 7 to 18 km (Fig. 15b and c, Poudjom Djomani et al. 1995). This suggests that the Congo Craton would have undergone repeated intrusions of crustal rock of a denser nature, which would have generated metacratonization processes during the Pan-African orogeny (Goussi Ngalamo et al. 2017) although the origin of this uplift is still unknown and stays under discussion. Otherwise, this uplift could be linked to the displacement of the African plate towards the north in a context of passive margin (e.g., Deffontaines et al. 2008) generated from the asthenospheric mantle (Lee et al. 1994). In this case, this resulted in the vertical thrust of the Moho observed in Central Africa since the opening of the South Atlantic to the Mesozoic. In several studies, relict landscapes and river anomalies produced by uplift processes as those observed in Kopongo were considered significant indicators (e.g., Clark et al. 2004). These same features were also found on the rivers of the southeastern margin of the Tibetan plateau, which show successive variations in the rate of rock uplift in space and time (Whipple 2004). By contrast, southwestern Cameroon shows a high rate of uplift in the context of passive margin, marked by several active faults and numerous active volcanic islands and complexes (Nsangou Ngapna et al. 2020) located within and near the Kopongo area. Kopongo region has been affected by active LF, NF, and SF (Moussango Ibohn et al. 2018; Nsangou Ngapna et al. 2020)

and KCSZ (Sandron et al. 2018) parallel and closer to the active CVL (Moudi et al. 2007; Kamgang et al. 2008). The UA is characterized by the highest uplift rates and lateral tilting (Figs. 7 and 8). This geometry observed along the margin and through time can also be related to the uplift and volcanic activities along the CVL. Consequently, the tectonic activities observed on Kopongo should be related to CVL. Otherwise, Owona (2008) suggested that the associated tectonic uplift of thickened crust defines the Nyong Group nappe that was transported top-to-the East towards the Ntem Group. Likewise, metagabbro rocks observed within the Nyong Group show decompression textures that can be explained by their rapid cooling and/or rapid uplift (Owona 2008). Thus, the existence of a regional relict landscape in the Kopongo area associated with a spatial variation of the relative tectonic uplift index (0.16–0.68), which is continuous with the Adamawa-Yade and West Cameroon domains, implies significant surface deformation (e.g., Clark et al. 2002; Goussi Ngalamo et al. 2017). Therefore, river anomalies (Fig. 7a and c) and landscape deformations such as normal (Fig. 7b–f) and inverse (Fig. 7b and g) dip-slip faults observed during field investigations reveal the influence of tectonic uplift.

Bs-values can be used to indicate the influence of the cartographic fold activities in the sub-watershed (Table 3; Fig. 11b). Their geometric shapes correspond mostly to cartographic folds described as polyharmonic  $F_{n+1}$  and  $F_{n+2}$



**Fig. 14** Map obtained at the Kopongo from geomorphic indices combination to illustrate the heterogeneity of relative tectonic activity index (IAT)



folds aligned as drap anticlines and shallow synclines with an asymmetric pattern (Abou’ou Ango et al. 2021).

The Vf and AF values enabled the detection of possible sub-basin tilt or differential uplift as well as the degree of the incision within the Kopongo area through different altitudinal classes (Table 5). The lower Vf-values ( $Vf < 1$ ) are observed in the IA and UA districts corresponding to narrow, steep, and deep V-shaped valleys, and characterizing a neotectonic that is marked by significant incision rate due to uplift processes. Meanwhile, high Vf-values ( $Vf > 1$ ) are displayed by LA district dominated by broad-floored (U-shape) canyons demonstrating an eroded area in a tectonically inactive environment (El Hamdouni et al. 2008; Ajay Kumar et al. 2017; Ajay Kumar et al. 2018). The intensity of the transverse tilt of a sub-watershed is determined by the AF-values (Ajay Kumar et al. 2020). The obtained values of AF all over the morphological units show a generalized asymmetry of the sub-basins, which could have a link with the tectonic tilting of the blocks

(Fig. 8d). To this end, the asymmetry of a sub-basin in an environment dominated by a progressive uplift can be linked to a structural orientation of the geological formations of the area (Alipoor et al. 2011). In the Kopongo area, four symmetric sub-watersheds are tectonically stable (SWs-I, V, VI, and XVII) with their AF-values close to 50 (Fig. 12), whereas a heterogeneity tectonic tilting towards the NW-W, NE-S, and SE directions is observed on the rest of sub-asymmetric to asymmetric sub-watersheds. This tectonic tilting is linked to their AF-values ( $AF < 50$  or  $AF > 50$ ), which indicate the response to uplift and/or influence of geological formations having experienced a tectonic deformation (Fig. 12c; Ajay Kumar et al. 2017). This shows an area dominated by thrust faults, whereby, the asymmetry of the sub-watershed developed during the tectonic displacement of tectonic blocks/Nyong Group nappes (Owona et al. 2011).

The spatial variability of the bifurcation ratio values displayed by sub-watersheds and the morphological units (i.e.,

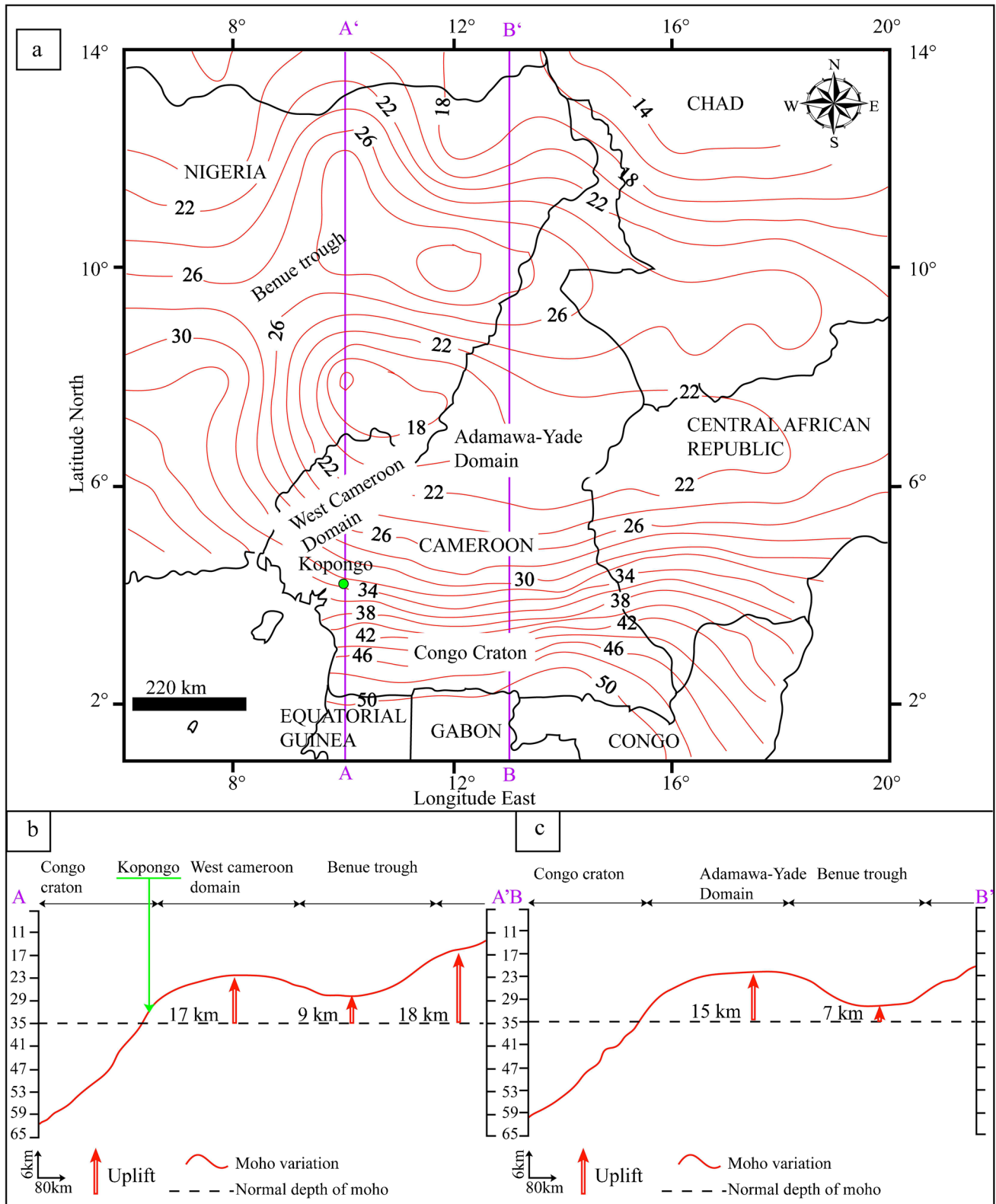


**Fig. 15** a Illustrative map of Moho depth (in km) of the Guinea gulf obtained from gravity data (after Poudjom Djomani et al. 1995). b and c Conceptual cross-sections of the northern edge of the Congo craton illustrating the crustal thickness variations along 10°N (AA') and 13°N (BB') latitude north



1.20–10.67) shows that the lithologic heterogeneity also influences the landscape evolution of this study area (Fig. 3, Sreedevi et al. 2004). Indeed, the lower Rb values observed within sub-watersheds show that there was a deep correlation with the high number of 1st and 2nd-order streams. Usually, moderate to high values of  $R_{bm} > 3$  in the Kopongo area were related to Loloma, Malibo, and Ngombe active faults and thrust fault activities (Fig. 13a) (e.g., Barman et al. 2021).

### Relative tectonic activity index interpretation

To evaluate the intensity of the active tectonic within the Kopongo region, the calculation of the Hi, U, Bs, AF, Rb, and Vf indices was applied. Their heterogeneity can be a consequence of the topography and drainage system changes influenced by faults and anticline growth activities (e.g., Jackson et al. 1998; Bahrami et al. 2020). Because the evolution of the reliefs is influenced by the growth of frontal anticlines, the topographic slopes thus created during this tectonic process impose a new drainage pattern (Keller and Pinter 1996). The topographic undulations observed at the Kopongo area shows that the growth of frontal anticlines was not constant and that regional folds displayed asymmetrical shapes due to active tectonic (Abou'ou Ango et al. 2021). In addition, the irregularity of their hinges shows that the basin areas were strongly eroded, while the dome areas were under the influence of strong tectonic activity (Abou'ou Ango et al. 2021). Besides, the regional  $F_n$ - $F_{n+2}$  folds generated were considered to be tectonic indicators emplaced from the W to E (Abou'ou Ango et al. 2021) during the thrust activities of the Nyong tectonic nappes over the Ntem Group (Feybesse et al. 1998). Later on, this area was overlaid by the Yaounde tectonic nappes, characterized by  $F_{n+3}$  nappe folds (Owona et al. 2011). Alternatively, these cartographic  $F_n$ - $F_{n+3}$  folds have been interpreted as anticlinal and synclinal (Tchameni et al. 2001) or as swell-and-basin-type (Poudjom Djomani et al. 1997) structures, with their geometrical disposition modified by sinistral normal faults (Fig. 7c). This variability of geomorphic indices, topographic surface parameters, structural features, frequency, and magnitude in the investigated area has served as indicators in other tectonically active regions (e.g., Mahmood and Gloaguen 2012; Ezati et al. 2021). Thus, the different values of IAT from the Kopongo area show that the explored area is more influenced by high to moderate tectonic activities. Thus, suggesting differences in relief and topographical features considered a consequence of the tectonic uplifts and tiltings (Figs. 7 and 8). This kind of tectonic activity level has been reported in the most active margins around the world (e.g., El Hamdouni et al. 2008; Melnick et al. 2009;

Ajay Kumar et al. 2020). It has also been linked to the following: (1) the variations in subduction zones (Clift and Vannucchi 2004) due to topographic anomalies, which would be closely related to the deduced decreasing uplift rate; (2) fold type variabilities such as fault-related folds, simple buckle folds, and fold following the old inherited fractures (Fouad 2010), e.g.,  $F_{n+onefold}$  crosscut by normal fault (Fig. 7c) and  $F_n$  fold overprinted by  $F_{n+1}$  folds (Fig. 7d); (3) the effects of rock uplift and rock resistance (e.g., Van Laningham et al. 2006), marked by a variability in lithological facies (Fig. 3); (4) crustal thickening (Rehak et al. 2008), which has not been observed within the study area (e.g., Poudjom Djomani et al. 1995); (5) uplift related to mantle plume in Cameroon that started around 34 Ma (Guillocheau et al. 2018) followed by a magmatic activity according to the alignment of the “plutonic-volcanic complexes” at ca.67 Ma to the present (Njonfang et al. 2011); and (6) climate changes (Miao et al. 2018) in rain forest from Late Cretaceous to Quaternary (Maley 1996), where the investigated area is located.

### Conclusion

Evaluation of the relative tectonic activity of the Kopongo area and the highlight of the main factors that controlled the evolution of this region end up with the following conclusions:

- (1) The Kopongo region is controlled by tectonics, climate, lithology, and mantle dynamics;
- (2) The region includes zones of low and high tectonic activities due to heterogeneous spatio-temporal distribution of uplift and tilting following the NE-SW direction;
- (3) The CVL is one of the main active geological features in Central Africa which constantly causes the uplift and tilting in the region.
- (4) Morphometric responses crossed with field data and drill cores support that the morphology of this portion of the southwestern Cameroon greenstone belt is the expression of the neotectonics that prevails in the region.

**Acknowledgements** This work represents an integrated part of the first author's thesis at the University of Yaounde I, which was supported and financed by the Compagnie Minière du Cameroun. The authors are grateful to the editors and anonymous reviewers for providing reviews and comments to improve this manuscript.

### Declarations

**Competing interests** The authors declare no competing interests.

## References

- Abou'ou Ango T, Njom B, Ekoa Bessa AZ, Onana JB, Bafon GT, Olinga J-B, Mvondo Ondo J (2021) Correlations between morphotectonic parameters and Precambrian tectonic structures in the Nyong Group greenstone belts: example of the Kopongo area (NW of the Congo Craton, Southwestern Cameroon). *J Afr Earth Sci* 182:104272
- Abou'ou Ango T, Njom B, Yannah M, Olinga J-B, Mvondo Ondo J (2022) Petrology, geochemistry and structural analysis of the Kopongo greenstone belt, Congo craton, southern Cameroon: geodynamic evolution and geotectonic styles. *Arabian J Geosci* 15:1518
- Ajay Kumar TP, Kumar CR, Avtar SJ, Bahadur SK, Akhtar A, Shashi GK, Rohit K, Vaibhav K, Sagarika R (2017) Active tectonic deformation along reactivated faults in Binta basin in Kumaun Himalaya of north India: inferences from tectono-geomorphic evaluation. *Z Geomorphol* 61:159–180
- Ajay Kumar T, Bahadur Singh K, Avtar Singh J, Ajay K, Akhtar A, Sadiq A, Beena K, Purushottam KG, Rajesh K, Anil Kumar S, Bhupinder S, Rakesh J (2018) Tectono-climatic influence on landscape changes in the glaciated Durung Drung basin, Zaskar Himalaya, India: a geospatial approach. *Quatern Int* 507:262–273
- Ajay Kumar T, Lalit MJ, Bahadur SK, Akhtar A, Girish CK, Raj SK, Anoop KS, Rakesh KD (2020) Tectonic imprints of landscape evolution in the Bhilangana and Mandakini basin, Garhwal Himalaya, India: a geospatial approach. *Quatern Int* 575–576:21–36
- Alipoor R, Poorkermani M, Zare M, El Hamdouni R (2011) Active tectonic assessment around Rudbar Lorestan dam site, High Zagros Belt (SW of Iran). *Geomorphology* 128:1–14
- Amine A, El Ouardi H, Zebari M, El Makrini H (2020) Active tectonics in the Moulay Idriss Massif (South Rifian Ridges, NW Morocco): new insights from geomorphic indices and drainage pattern analysis. *J Afr Earth Sci* 167:103833
- Ateba B, Ntepe N, Ekodeck GE, Soba D, Fairhead JD (1992) The recent earthquakes of South Cameroon and their possible relationship with main geological units of central Africa. *J Afr Earth Sci* 14:365–369
- Bahrami S, Capolongo D, Mofrad MR (2020) Morphometry of drainage basins and stream networks as an indicator of active fold growth (Gorm anticline, Fars Province, Iran). *Geomorphology* 355:107086
- Bamford MK (2000) Cenozoic macro-plants. In: Partridge TC, Maud RR (eds) *The Cenozoic of southern Africa*. Oxford University Press, Oxford, pp 351–356
- Barman BK, Rao CU B, Srinivasa Rao K, Patel A, Kushwaha K, Singh SK (2021) Geomorphic analysis, morphometric-based prioritization and tectonic implications in Chite Lui River, Northeast India. *J Geol Soc India* 97:385–395
- Bathrellos GD, Antoniou VE, Skilodimou HD (2009) Morphotectonic characteristics of Lefkas Island during the Quaternary (Ionian Sea, Greece). *Geologica Balcanica* 38:23–33
- Benkhelil J, Robineau B (1983) Le fossé de la Bénoué est-il un rift? *Bull Centres Recherches Expl Prod Elf Aquitaine* 7:315–321
- Bouyo Houketchang BM, Penaye J, Mouri H, Toteu SF (2019) Eclogite facies metabasites from the Paleoproterozoic Nyong Group, SW Cameroon: mineralogical evidence and implications for a high-pressure metamorphism related to a subduction zone at the NW margin of the Archean Congo craton. *J Afr Earth Sci* 149:215–234
- Burbank DW, Anderson RS (2001) *Tectonic Geomorphology*. Blackwell Science, Oxford, p 247
- Burke K, Gunnell Y (2008) The African erosion surface: a continental-scale synthesis of geomorphology, tectonics, and environmental change over the past 180 million years. *Geol Soc Am Mem* 201:66p
- Castaing C, Feybesse JL, Thiéblemont D, Triboulet C, Chèvremont P (1994) Palaeogeographical reconstructions of the Pan-African/Brasiliano orogen: closure of oceanic domain or intracontinental convergence between major blocks. *Precambrian Res* 69:327–344
- Chombong NN, Suh CE (2013) 2883 Ma commencement of BIF deposition at the northern edge of Congo craton, southern Cameroon: new zircon SHRIMP data constraint from meta-volcanics. *Episodes* 36:47–57
- Chow Ven T (1964) *Handbook of applied hydrology*. McGraw Hill Inc, New York
- Clark MK, Royden LH, Burchfiel BC, Whipple KX, House MA, Zhang X (2002) Preservation of a low-relief, regionally continuous erosion surface in southeastern Tibet: evidence for the transient condition of the southeastern plateau margin: *Geological Society of America Abstracts with Programs* 34(6):411
- Clark MK, Schoenbohm LM, Royden LH, Whipple KX, Burchfiel BC, Zhang X, Tang W, Wang E, Chen L (2004) Surface uplift, tectonics and erosion of eastern Tibet from large-scale drainage patterns: *Tectonics* 23:TC1006
- Clift P, Vannucchi P (2004) Controls on tectonic accretion versus erosion in subduction zones: implications for the origin and recycling of the continental crust. *Rev Geophys* 42:RG2001
- Cornacchia M, Dars R (1983) Un trait structural majeur du continent africain. Les linéaments centrafricains du Cameroun au Golfe d'Aden. *Bull Soc Géol France* 7:101–109
- Dana JD (1856) On American geological history: 1856. *Am J Sci* 22:305–344
- De Almeida FFM, Hasui Y, De Brito Neves BB, Frick RA (1981) Brazilian structural provinces: an introduction. *Earth Sci Rev* 17:1–29
- Deffontaines B, Ben Hassen M, Slama T, Rebai N, Turki MM (2008) Tunisian structural extrusion revealed by numerical geomorphometry. In: Brady SR, Sinha AK, Gundersen LC (eds) *Geoinformatics 2008-data to knowledge*, proceedings, geoinformatics 2008-Data to knowledge. USGS, Reston, VA, pp 14–15
- Déruelle B, Ngounounou I, Demaiffe D (2007) The “Cameroon Hot Line” (CHL): a unique example of active alkaline intraplate structure in both oceanic and continental lithospheres. *CR Géosci* 339:589–600
- Dorbath C, Dorbath L, Fairhead D, Stuart GW (1986) A teleseismic delay time study across the Central African Shear Zone in the Adamawa Region of Cameroon, West Africa. *Geophys J Int* 86:751–766
- Dumont JF (1986) Identification par télédétection de l'accident de la Sanaga (Cameroun). Sa position dans le contexte des grands accidents d'Afrique Centrale et de la limite nord du craton concolais. *Géodynamique* 1:13–19
- Ebah Abeng SA, Ndjigui P-D, Beyanu AA, Bilong P (2012) Geochemistry of pyroxenites, amphibolites and their weathered products in the Nyong unit, SW Cameroon (NW border of Congo Craton): implications for Au PGE exploration. *J Geochem Explor* 114:1–19
- El Hamdouni R, Irigaray C, Fernández T, Chacón J, Keller EA (2008) Assessment of relative active tectonics, southwest border of the Sierra Nevada (southern Spain). *Geomorphology* 96:150–173
- Ezati M, Gholami E, Mousavi SM (2021) Tectonic activity level evaluation using geomorphic indices in the Shekarab Mountains Eastern Iran. *Arabian J Geosci* 14:385
- Feybesse JL, Johan V, Triboulet C, Guerrot C, Mayaga-Mikolo F, Bouchot V, Eko N'dong J (1998) The West Central African belt: a model of 2.5–2.0 Ga accretion and two-phase orogenic evolution. *Precambrian Res* 87:161–216
- Fouad SF (2010) Tectonic evolution of the Mesopotamia Foredeep in Iraq. *Iraqi Bull Geol Min* 6(2)
- Fuh CG, Nkoumbou C, Tchakounte Numbem J, Mukete KO, Tchouankou JP (2021) Petrology, geochemistry, Ar/Ar isotopes of an arc-related calc-alkaline pluton from Mamb (Pan-African Yaounde



- group, Cameroon): a testimony to the subduction of a hot oceanic crust. *Lithos* 384–385:105973
- Gaëlle Nana V, Lepatio Tchieg SA, Ntomb Biboum EO, Fosso Tegua EEM, Nguiya S, Tokam Kamga AP (2021) Preliminary study of seismic hazard along the Cameroon Volcanic Line. *Am J Earth Sci* 8:1–10
- Goussi Ngalamo JFG, Bisso D, Abdelsalam MG, Atekwana EA, Katumwehe AB, Ekodeck GE (2017) Geophysical imaging of metacratonization in the northern edge of the Congo craton in Cameroon. *J Afr Earth Sc* 129:94–107
- Grimaud JL (2014) Dynamique long terme de l'érosion en contexte cratonique: l'Afrique de l'Ouest depuis l'Eocène. *Géoscience Université de Toulouse France*
- Grohmann CH (2004) Morphometric analysis in geographic information systems: applications of free software GRASS and R. *Computers Et Geosci* 30:1055–1067
- Guillocheau F, Simon B, Baby G, Bessin P, Robin C, Dauteuil O (2018) Planation surfaces as a record of mantle dynamics: the case example of Africa. *Gondwana Res* 53:82–98
- Gu ZK, Shi CX (2018) Dynamical characteristics of geomorphologic evolution of the basins covered by Pishasandstone in the eastern wing of the Ordos Plateau, China. *J Mt Sci* 15(5)
- Hay WW, Soeding E, DeConto RM, Wold CN (2002) The Late Cenozoic uplift – climate change paradox. *Int J Earth Sci (geol Rundsch)* 91:746–774
- Jackson J, Van Dissen R, Berryman K (1998) Tilting of active folds and faults in the Manawatu region, New Zealand: evidence from surface drainage patterns, New Zealand. *J Geol Geophys* 41:377–385
- Jenness JS (2013) DEM Surface Tools for ArcGis (surface\_area.exe). Calculating landscape surface area from digital elevation models. *Wildl Soc Bull* 32:829–839
- Kamgang P, Chazot G, Njonfang E, Tchoua F (2008) Geochemistry and geochronology of mafic rocks from Bamenda Mountains (Cameroon): source composition and crustal contamination along the Cameroon Volcanic Line. *CR Geosci* 340:850–857
- Keller A, Pinter N (1996) Active tectonics, earthquakes, uplift and landscape. *Prebtuce-Hall, Inc Simon and Schuster*, pp 1–237
- Keller EA, Pinter N (2002) Active tectonics. *Earthquakes, Uplift, and Landscape*, 2<sup>nd</sup> edn. Prentice-Hall, Upper Saddle River, p 362
- Kirby E, Whipple KX (2012) Expression of active tectonics in erosional landscapes. *J Struct Geol* 44:54–75
- Klimaszewski M (1978) *Geomorphology (in Polish)*. PWN Warszawa
- Koum S, Mvondo Owono F, Ntamak-Nida MJ, Njom B, Essama Boum RB (2013) Surrection relative plio-pléistocène de la surface côtière de la marge sud du Rio Del Rey (Cameroon) à partir de la géomorphologie quantitative sur Modèle Numérique de Terrain (MNT). *Sci Technol Et Dév* 14:59–69
- Lasserre M, Soba D (1976) Age libérien des granodiorites et des gneiss à pyroxène du Cameroun méridional. *Bulletin du Bureau de Recherches Géologiques et Minières; Section 4: Geologie Generale*, pp 17–32
- Lee DC, Halliday AN, Fitton GJ, Poli G (1994) Isotopic variations with distance and time in the volcanic islands of the Cameroon Line: evidence of the mantle plume origin. *Earth Planet Sci Lett* 123:119–138
- Ledru P, Johan V, Milesi JP, Tegye M (1994) Markers of the last stages of the Palaeoproterozoic collision: evidence for a 2 Ga continent involving circum-South Atlantic provinces. *Precambrian Res* 69:169–191
- Lerouge C, Cocherie A, Toteu SF, Milesi JP, Penaye J, TchameniR NNE, Fanning CM (2006) Shrimp U/Pb zircon age evidence for Paleoproterozoic sedimentation and 2.05Ga syntectonic plutonism in the Nyong Group, southwestern Cameroon: consequences for the Eburnean-Transamazonian belt of NE Brazil and central Africa. *J Afr Earth Sci* 44:413–427
- Loose D, Schenk V (2018) 2.09 Ga old eclogites in the Eburnian-Transamazonian orogen of southern Cameroon: significance for Palaeoproterozoic plate tectonics. *Precambrian Res* 304:1–11
- Mahmood SA, Gloaguen R (2012) Appraisal of active tectonics in Hindu Kush: insights from DEM derived geomorphic indices and drainage analysis. *Geosci Front* 3:407–428
- Maley J (1996) The African rain forest- main characteristics of changes in vegetation and climate from the Upper Cretaceous to the Quaternary. *Proc de Royal Soc Edinburgh* 1048:31–73
- Maurizot P, Abessolo A, Feybesse J, Johan L, Lecomte P (1986) Etude et prospection minière du Sud-Ouest du Cameroun : synthèse des travaux de 1978 à 1985. *Rapport BRGM 85 CMR 066*, p 274
- Melnick D, Bookhagen B, Strecker MR, Echtler HP (2009) Segmentation of megathrust rupture zones from fore-arc deformation patterns over hundreds to millions of years, Arauco peninsula, Chile. *J Geophys Res* 114:B01407
- Miao Y, Warny S, Clift PD, Gregory M, Liu C (2018) Climatic or tectonic control on organic matter deposition in the South China Sea? A lesson learned from a comprehensive Neogene palynological study of IODP Site U1433. *Int J Coal Geol* 190:166–177
- Minyem D (1994) Contribution à l'étude métamorphique et structurale du secteur Eséka-Makak (Cameroun, Département de Nyong et kélé), Thèse de 3<sup>e</sup> cycle. *Univ Ydé I:166p*
- Moudi A, Wandji P, Bardintzeff J-M, Ménard J-J, Okomo Atouba LC, Reusser E, Bellon H, Tchoua MF (2007) Les basaltes éocènes à affinité transitionnelle du plateau Bamoun, témoins d'un réservoir mantellique enrichi sous la ligne volcanique du Cameroun. *CR Geosci* 339:396–406
- Moussango Ibohn AP, Owono FM, Njom B, Mbog Bassong SP, Sep Nlomngan JP, Sébastien Owona S, Ekodeck EG (2018) Sanaga fault: evidence of neotectonics and landscape evolution in Edéa Region (Cameroon, Centre-Africa). *J Geography Geol* 10:7
- Mvondo Owono F (2011) Surrection cénozoïque des marges passives de l'Ouest d'Afrique à partir de deux exemples: le plateau sud Namibien et la marge nord camerounaise. *Th Doc Pub Univ Rennes 1 France*
- Mvondo Owono F, Ntsama Atangana J, Owona S, Dauteuil O, Nsangou Ngapna M, Guillocheau F, Koum S, Essama Boum RB, Ntamak Nida MJ (2022) Tectono-stratigraphic evolution and architecture of the Miocene Rio del Rey basin (Cameroon margin, Gulf of Guinea). *Int J Earth Sci* 109:2557–2581
- Ndam Ngoupayou JR, Kpoumie A, Boeglin J-L, Lienou G, Nfocco AK, Ekodeck GE (2007) Transports solides et érosion mécanique dans un écosystème tropical d'Afrique: exemple du bassin versant de la Sanaga au Sud-Cameroun. *Actes des JSIRAUF, Hanoi*
- Ndema Mbongue J, Ngo Nlend CD, Nzenti JP, Cheo Suh E (2014) Origin and evolution of the formation of the Cameroon Nyong Series in the Western Border of the Congo Craton. *J Geosci Geomat* 2:62–75
- Ndibi EDD, Mbossi EF, Wokwenmendang NP, Ateba B, Ndoungsa-Mbarga T (2021) Probabilistic seismic hazard assessment for the main cities along the continental section of the Cameroon Volcanic Line. *Arab J Geosci* 14:796
- Ndikum EN, Tabod CT, Tokam APK, Essimbi BZ (2014) Fault-plane solution of the earthquake of 19 March 2005 in Monatele (Cameroon). *Open J Geol* 4(6):47140
- Nfoumou N, Tongwa AF, Ubangoh RU, Ateba B, Nnange JM, Hell JV (2004) The July 2012 earthquake in the Kribi region: geological context and preliminary evaluation of seismic risk in southwestern Cameroon. *J Afr Earth Sci* 40:163–172
- Ngako V, Jegouzo P, Nzenti JP (1991) Le Cisaillement Centre Camerounais. Rôle structural et géodynamique dans l'orogénèse panafricaine. *CR Acad Sci Paris* 313:457–463
- Ngako V, Affaton P, Nnange JM, Njanko T (2003) Pan-African tectonic evolution in central and southern Cameroon: transpression and transtension during sinistral shear movements. *J Afr Earth Sci* 36:207–214

- Ngako V, Affaton P, Njonfang E (2008) Pan-African tectonics in north-western Cameroon: implication for the history of western Gondwana. *Gondwana Res* 14:509–522
- Ngatchou HE, Nguiya S, Owona Angue MLC, Mouzoug PM, Tokam AP (2018) Source characterization and tectonic implications of the M 4.6 Monatele (Cameroon) earthquake of 19 March 2005. *S Afr J Geol* 121:191–200
- Njome MS, De Wit MJ (2014) The Cameroon line: analysis of intra-plate magmatic province transecting both oceanic and continental lithospheres: constraints, controversies and models. *Earth Sci Rev* 139:168–194
- Njonfang E, Nono A, Kamgang P, Ngako V, Tchoua F (2011) Cameroon Line alkaline magmatism (Central Africa): a reappraisal. *Geol Soc Am* 478:173–191
- Nkouathio DG, Kagou Dongmo A, Bardintzeff J-M, Wandji P, Bellon H, Pouclet A (2008) Evolution of volcanism in graben and horst structures along the Cenozoic Cameroon Line (Africa): implications for tectonic evolution and mantle source composition. *Mineral Petrol* 94:287–303
- Noel EOP, Marcelin MP, Bekoa A (2014) Crustal structure and seismogenic zone of Cameroon: integrated seismic, geological and geophysical data. *Open J Earthq Res* 3:152–161
- Nsangou Ngapna M, Owona S, Owono F M, Ateba CB, Tsimi VM, Mvondo Ondo J, Ekodeck GE (2020) Assessment of relative active tectonics in Edea - Eseka region (SW Cameroon, Central Africa). *J Afr Earth Sc* 164:103798
- Olivry JC (1986) Fleuve et rivière du Cameroun. Collection “Monographie hydrographie” ORSTOM, N°9, Paris
- Owona S (2008) Archaean, Eburnean and Pan-African features and relationships in their junction zone in the South of Yaoundé (Cameroon). Ph.D. Thesis. University of Douala, Cameroon, p 232
- Owona S, Mvondo Ondo J, Ratschbascher L, Mbola Ndzana SP, Tchoua MF, Ekodeck GE (2011) The geometry of the Archaean, Paleo and Neoproterozoic tectonics in Southwest Cameroon. *C.R. de l'Acad des Sci* 343:312–322
- Penaye J, Toteu SF, Tchameni R, Van Schmus WR, Tchakounte J, Ganwa A, Miyem D, Nsifa EN (2004) The 2.1 Ga West Central African Belt in Cameroon: extension and evolution. *J Afr Earth Sci* 39:159–164
- Pérez-Peña JV, Azañón JM, Azor A (2009) CalHypso: an ArcGIS extension to calculate hypsometric curves and their statistical moments. Applications to drainage basin analysis in SE Spain. *Comput Geosci* 35:1214–1223
- Pérez-Peña JV, Azor A, Azañón JM (2010) Active tectonics in the Sierra Nevada (Betic Cordillera, SE Spain): insights from geomorphic indices and drainage pattern analysis. *Geomorphology* 119:74–87
- Pérez-Peña JV, Al-Awabdeh M, Azañón JM, Galve JP, Booth-Rea G, Notti D (2016) SwathProfiler and NProfiler: two new ArcGIS Add-ins for the automatic extraction of swath and normalized river profiles. *Comput Geosci*. <https://doi.org/10.1016/j.cageo.2016.08.008>
- Pickford M, Senut B (1999) The geological and faunal context of Late Miocene hominid remains from Lukeino, Kenya. *C.R. Acad Sci Paris* 332:145–152
- Poudjom Djomani Y, Nnange J, Diament M, Ebinger C, Fairhead J (1995) Effective elastic thickness and crustal thickness variations in west central Africa inferred from gravity data. *J Geophys Res: Solid Earth* 100:22047–22070
- Poudjom Djomani YH, Diament M, Wilson M (1997) Lithospheric structure across the Adamawa Plateau (Cameroon) from gravity studies. *Tectonophysics* 273:317–327
- Regard V, Carretier S, Boeglin JL, Ndam Ngoupayou JR, Dzana JG, Bedimo Bedimo JP, Riotte J, Braun JJ (2016) Denudation rates on cratonic landscapes: comparison between suspended and dissolved fluxes, and <sup>10</sup>Be analysis in the Nyong and Sanaga River basins, South Cameroon. *Earth Surf Process Landforms* 41:1671–1683
- Rehak K, Strecker MR, Echtler HP (2008) Morphotectonic segmentation of an active forearc, 37–41S, Chile. *Geomorphology* 94:98–116
- Sandron D, Santulin M, Tamaro A, Orzi C, Benedetti G, Castellaro S, Romeo R, Rebez A, Grimaz S, Malisan P, Guadagnini G, Sciascia F, Slejko D (2018) Seismic parameter design assessment for the Kribi deep seaport in Cameroon. *Bull Earthq Eng* 17:1825–1861
- Ségalen P (1967) Les sols et la géomorphologie du Cameroun. *Cah. Off. Rech. Sci. Techn. Outre-Mer. Sér Pédol* 2:137–187
- Sighomnou D (2004) Analyse et redéfinition des régimes climatiques et hydrologiques du Cameroun : perspective d'évolution des ressources en eau. Th. Doc. Etat Univ, Ydé I, p 289
- Sreedevi PD, Subrahmanyam K, Ahmed S (2004) The significance of morphometric analysis for obtaining groundwater potential zones in a structurally controlled terrain. *Environ Geol* 47:412–420
- Strahler A (1952) Hypsometric (area altitude) analysis of erosional topology. *Geol Soc Am Bull* 63:1117–1142
- Strahler AN (1957) Quantitative analysis of watershed geomorphology. *Trans Am Geophys Union* 38:913–920
- Tabot CT, Fairhead JD, Stuart GW, Ateba B, Ntepe N (1992) Seismicity of the Cameroon Volcanic Line, 1982–1990. *Tectonophysics* 212:303–320
- Tchameni R, Mezger K, Nsifa NE, Pouclet A (2001) Crustal origin of Early Proterozoic syenites in the Congo craton (Ntem complex), South Cameroon. *Lithos* 57:23–42
- Tchindjang M, Levang P, Saha F, Voundi E, Njombissié Petchou IC (2015) Impact et suivi par télédétection du développement des plantations villageoises de palmiers à huile sur le couvert forestier au Cameroun : cas de la Sanaga Maritime (3°20–4°40N, 9°30–11°20E). Yaoundé, PALMFORCAM : Rapport Principal (37p) et Rapport annexes, p 123
- Teixeira W, Figueiredo MCH (1991) An outline of early-Proterozoic crustal evolution in the Saõ Francisco craton, Brazil: a review. *Precamb Res* 53:1–22
- Toteu SF, Macaudiere J, Bertrand JM, Dautel D (1990) Metamorphic zircons from North Cameroon; implications for the Pan-African evolution of central Africa. *Geol Rundsch* 79:777–788
- Toteu SF, Van Schmus WR, Penaye J, Nyobe JB (1994) U-Pb and Sm-Nd evidence for Eburnean and Pan-African high-grade metamorphism in cratonic rocks of southern Cameroon. *Precambrian Res* 67:321–347
- Van Laningham S, Meigs A, Goldfinger C (2006) The effects of rock uplift and rock resistance on river morphology in a subduction zone forearc, Oregon, USA. *Earth Surf Process Landforms* 31:1257–1279
- Van Schmus WR, Oliveira EP, Da Silva Filho AF, Toteu SF, Penaye J, Guimarães IP (2008) Proterozoic links between the Borborema province, NE Brazil, and the central-African Fold belt. *Geol Soc London* 294:69–99
- Weber F, Gauthier-Lafaye F, Whitechurch H, Ulrich M, El Albani A (2016) The 2-Ga Eburnean Orogeny in Gabon and the opening of the Francevillian intracratonic basins: a review. *Compt Rendus Geosci* 348:572–586
- Whipple KX (2004) Bedrock Rivers and the geomorphology of active orogens. *Annu Rev Earth Planet Sci* 32:151–185

Springer Nature or its licensor (e.g. a society or other partner) holds exclusive rights to this article under a publishing agreement with the author(s) or other rightsholder(s); author self-archiving of the accepted manuscript version of this article is solely governed by the terms of such publishing agreement and applicable law.